Accuracy of the new feed positioning system of GMRT from observations of calibrator sources

Subhashis Roy, Santaji N. Katore & Shailendra K. Bagde

September 22, 2023

NCRA-TIFR
Pune-7

1 Introduction

Accuracy of the old Feed Positioning System (FPS) was quite limited, which could introduce an error in feed position from the target by up to half a degree (at the quadripod). This used to result in antenna based offset of a few arc-minutes (ratio of feed rotation offset to antenna pointing offset is 10:1 for GMRT). Moreover, it was incremental and needed a reference position to measure present feed position. The new FPS system has now replaced the older ones in all the antennas. It provides absolute angle, and its accuracy is expected to be $\sim 1'$.

This is an update on the pointing accuracy of the new FPS system based on pointing offset measurements with calibrators used in radio interferometric observations. These tests were meant to check if the new FPS system can provide reliable feed position, so that pointing accuracy is not affected due to rotation of feed positioning system during selection of new observing band. If these tests are satisfactory, we could save the time needed for antenna pointing after each feed rotation (**$\sim$300 hours** in an observing cycle). In first part of these tests, we present results from four different epochs of testing. During these tests, pointing scans were taken using band-5 ($\sim$ 1.4 GHz) feeds rotated towards the antenna apex. Then, the feeds were rotated to a different band, and were rotated back for band-5 observations. The pointing scans were repeated in band-5. In the second part of the tests, we carried out pointing tests on each Thursday morning (during maintenance slot) in band-5 after loading fixed offsets (measured at the 1st day of the 2 epochs) for each antennas.

2 Observations:

2.1 Feed rotations followed by grid pointing

For the 1st part of the the tests, the following method was used. Band-5 feeds were pointed towards antenna apex, then feed positioning system (FPS) were rotated to select a different band for observation, and then FPS was rotated back to point band-5 feeds towards antenna apex. If the FPS accurately points a feed of a particular band along the antenna axis, astronomical pointing offsets of the antennas should not change with feed rotations.

Here, astronomical offsets of the antennas were measured either using raster-scans or grid-pointing. In the case of **raster scans**, antennas are rotated (e.g., in elevation) at a fixed rate to reach zero-offset at a particular time after starting of rotation with a fixed offset. The difference of observed time to peak from the expected time along with the known angular speed of antenna rotation is used to determine their offsets in elevation (or in azimuth). In the case of **grid-pointing**, a calibrator is observed with 5 to 9 known offsets for ~ 1 minute at each grid points either in elevation or azimuth. The source offsets change from one grid point to the next and the maximum offset is about the FWHM of the antenna primary beam. A Gaussian curve is then fitted to the offsets vs antenna gain to determine antenna based offsets. We note that no pointing model was applied during these tests.

Details of the first part of the tests based on feed rotations were are given below:
On **30th Nov** 2021, feed rotations to band-5 followed by elevation pointing were done on the calibrator 1822-096 after transit, and there were 5 successive feed rotation from and back to 1.4 GHz band. Grid-pointing in elevation was done after each time the 1.4 GHz feeds were pointed towards the antenna apex.

The tests on **20th Dec** were done on the calibrator 3C48 before transit and there were 7 successive feed rotation from and back to 1.4 GHz band. Grid-pointing in elevation was done after each time the 1.4 GHz feeds were pointed towards the apex of each antenna.

The tests on **22th Dec** were done on the calibrator 3C286 before transit with 4 successive feed rotation from band-5 to other bands and back to the same band. Grid-pointing in elevation was done after each time the 1.4 GHz feeds were pointed towards the antenna apex. Another two such band-5 feed rotations followed by elevation raster-scan were done on the calibrator 1459+716 before transit.

The last scan on 1459+716 was not done properly, and is not shown in the plots.

The tests on **25th Dec** 2021 were done on the calibrator 3C286 after transit and there were 7 successive feed rotation from and back to 1.4 GHz band followed by grid-pointing.

2.2 Weekly pointing offsets with fixed offsets

In the 2nd part of the test, grid-pointing with the new TGC was used to observe a known calibrator every Thursday morning at about the same time using the L-band. As feeds are rotated multiple times during an week of observation with different bands, observing a fixed source every week will show if there is a measurable jitter in antenna offsets due to these feed rotations. This calibrator was chosen to be with a negative declination, such that its elevation angle variation over $\sim 2-3$ months of observations do not change by $\gtrsim 30^\circ$. As elevation difference cause the bulk of pointing errors, this minimises systematic pointing offsets caused by antenna dependent factors. These were done during May−July 2022 on the calibrator 2137−207 and November 2022 to February 2023 on the calibrator 1130−148. The dates of the test observations and the corresponding azimuth and elevation angles of the calibrator (within parenthesis in degrees) are given below.
(i) May to July 2022: 05 (147, 43), 12 (153, 46), 19 (164, 49), 26th (172, 50) May; 02 (-161, 48), 09 (-152, 45), 16 (-156, 47), 23rd (-145, 42) June; 07 (-140, 39), 14 (-131, 32), 21 (-128, 29) and 28th (-121, 19) July respectively.
(ii) November 2022 to February 2023: 17th (128, 38) Nov; 01 (135, 44), 08 (154, 52), 22 (-170, 55), 29th (178, 56) December; 05 (-169, 55), 12 (-144, 49), 26th (-133, 42) January; 02 (-130, 40), 09 (-128, 38), 16 (-120, 28) and 23rd (-119, 27) February. Observations did either fail or or was not done as intended for the Thursdays missing within the above date ranges. Among these observations, the 1st one (17th Nov) was used to determine the fixed offsets for the antennas, and is not shown in plots (Section 3.2.2).

3 Results:

3.1 Feed rotations in four different epochs

Attached are the plots (Figs. 1−29) of pointing offset as a function of time (elevation angle of the calibrators have been marked for each point), with elevation offsets determined by using grid-pointing in elevation. Plots for each of the antennas for the four days of observations have been shown on each page. The type of FPS system (old or new FPS encoder used) and the the date of observation are written in the title of each plot. The 2 different colours used in the plots are for 2 different polarisations.

On 30th Nov and 25th Dec 2021, the variation of elevation angles during the feed rotations were less than 35°. For these days, except C11 (Fig. 10) & W01 (Fig. 24) on 30th Nov, and W03 (Fig. 26) & W06 (Fig. 29) on 25th Dec, change in antenna based elevation offsets involving antennas with new FPS systems remained within $\sim 1'$ from their mean positions. The 3rd scan with C11 on 30 Nov clearly showed large deviation ($\sim 10'$) {see Fig. 10}, where grid-pointing plot did not show any obvious problem in fitting a Gaussian curve to data (Fig. 30). This appears to be from a genuine problem in feed positioning, as no acknowledgement of successful positioning was received from the antenna in this case. The feed was supposed to be manually positioned in this case, which was not done. The plot of grid-pointing on the 2nd scan (not shown here) of W01 showed fitting problem (Fig. 24). Therefore, it was not related to any issue with the new FPS system. On 25th Dec, W03 showed significant systematic pointing offset as source elevation decreased (Fig. 26). As feed positioning error is expected to be random in nature, systematic change in offset with elevation indicates antenna pointing error due to gravitational bending. W06 elevation offset has been observed

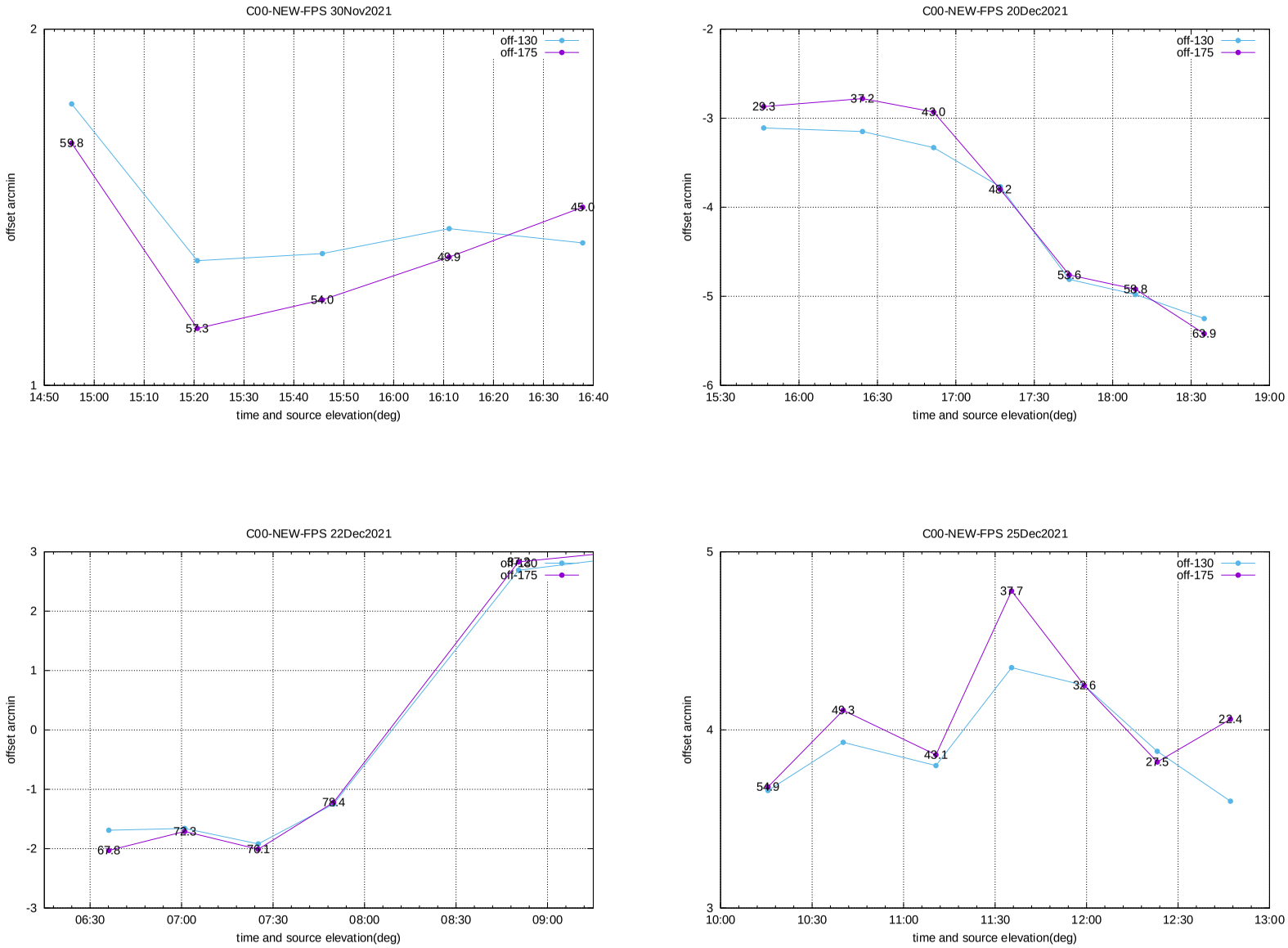

Antenna elevation offset as a function of time and elevation (shown against each points).

Figure 1: Elevation offsets after each `feed-rotation`.

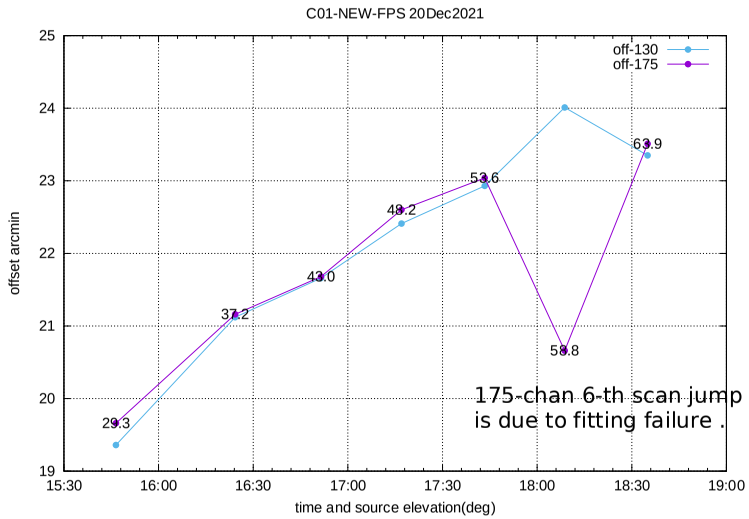

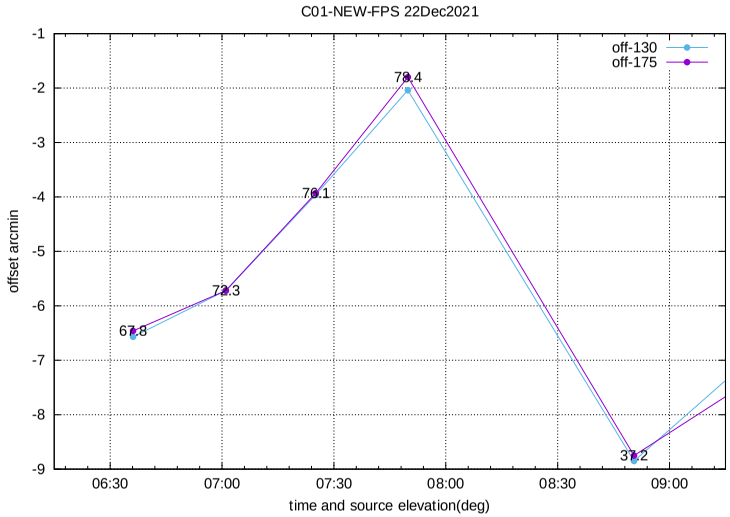

Antenna elevation offset as a function of time and elevation (shown against each points).

Figure 2: Elevation offsets after each `feed-rotation`.

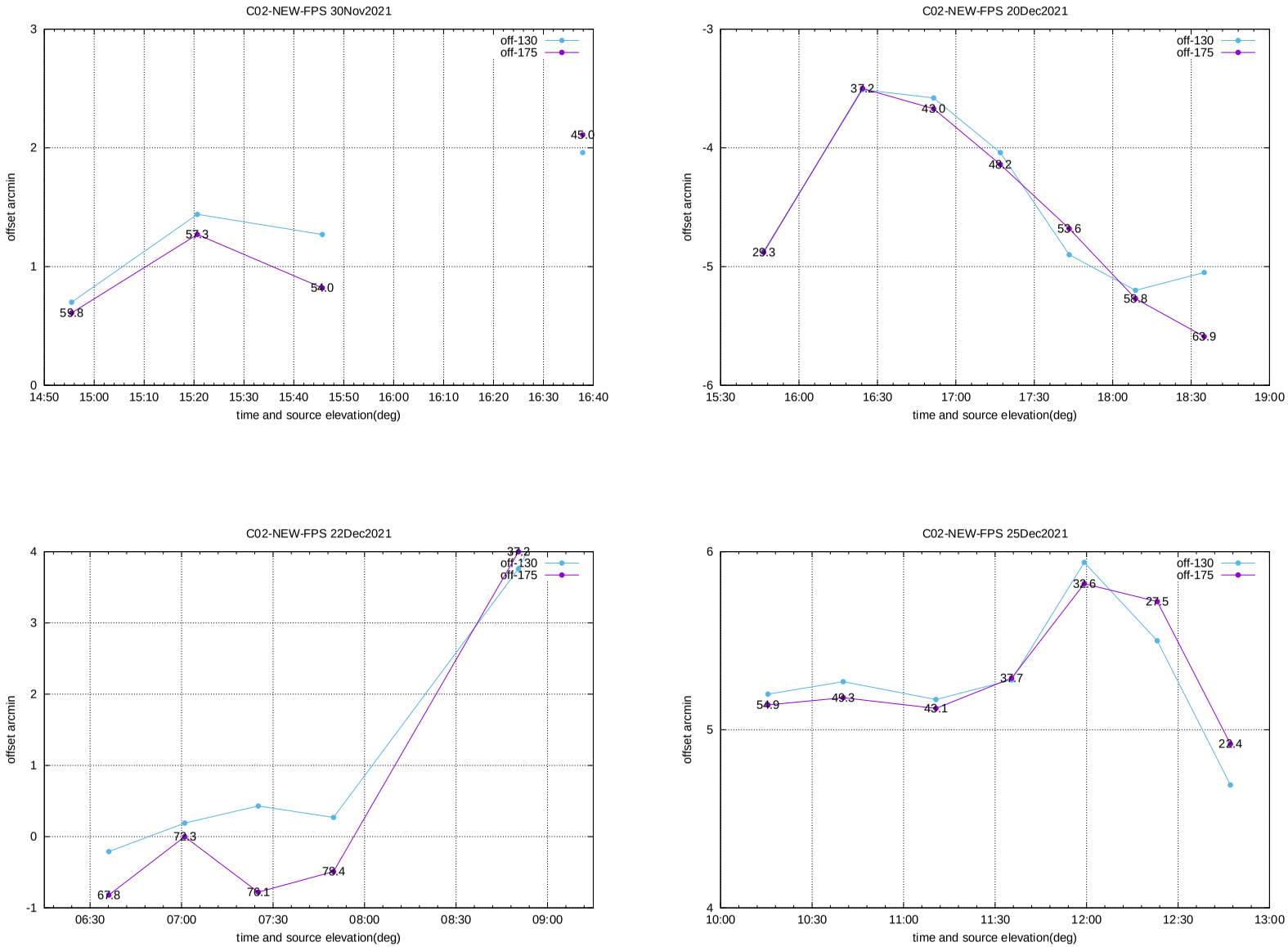

Antenna elevation offset as a function of time and elevation (shown against each points).

Figure 3: Elevation offsets after each `feed-rotation`.

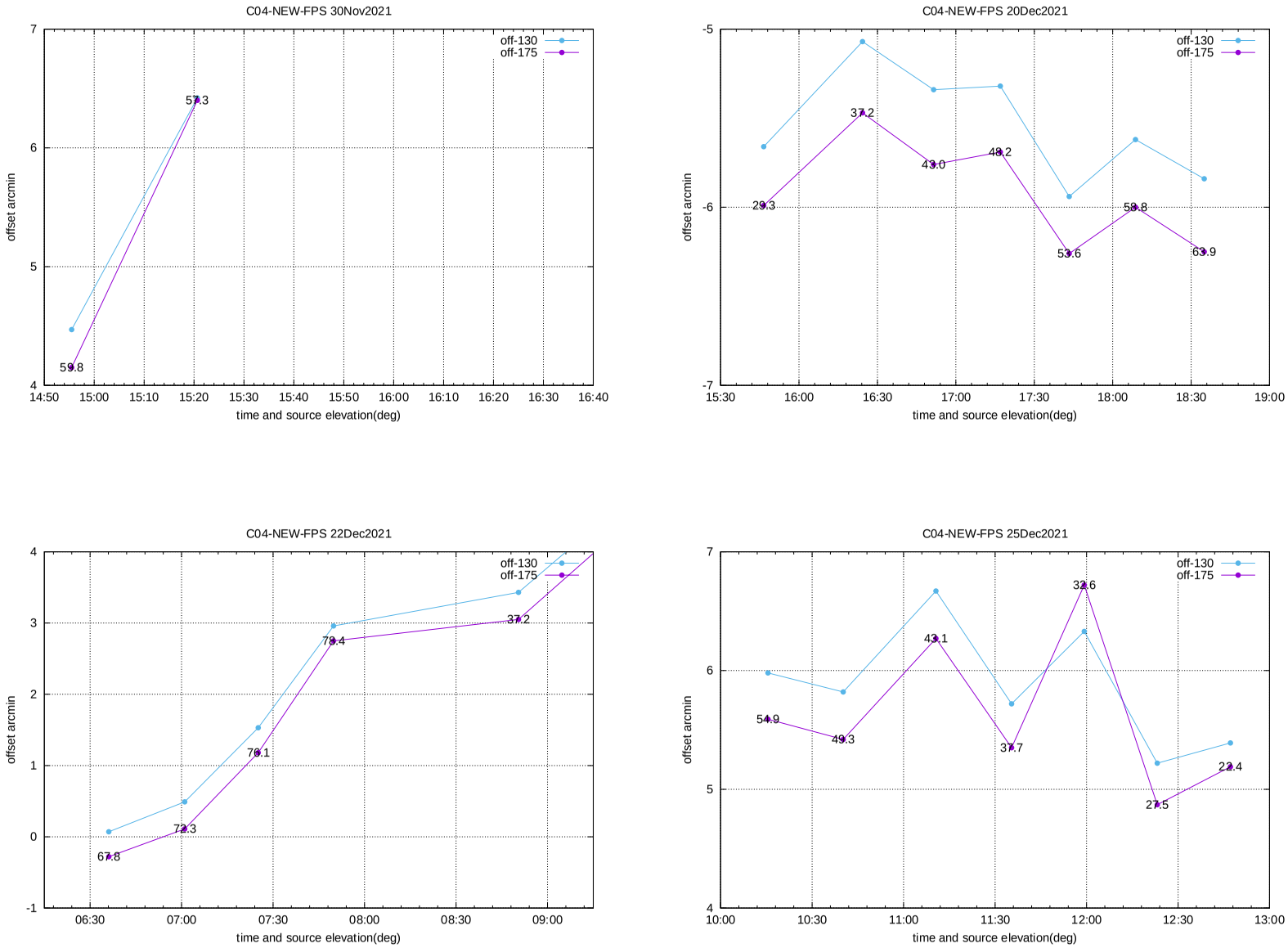

Antenna elevation offset as a function of time and elevation (shown against each points).

Figure 4: Elevation offsets after each `feed-rotation`.

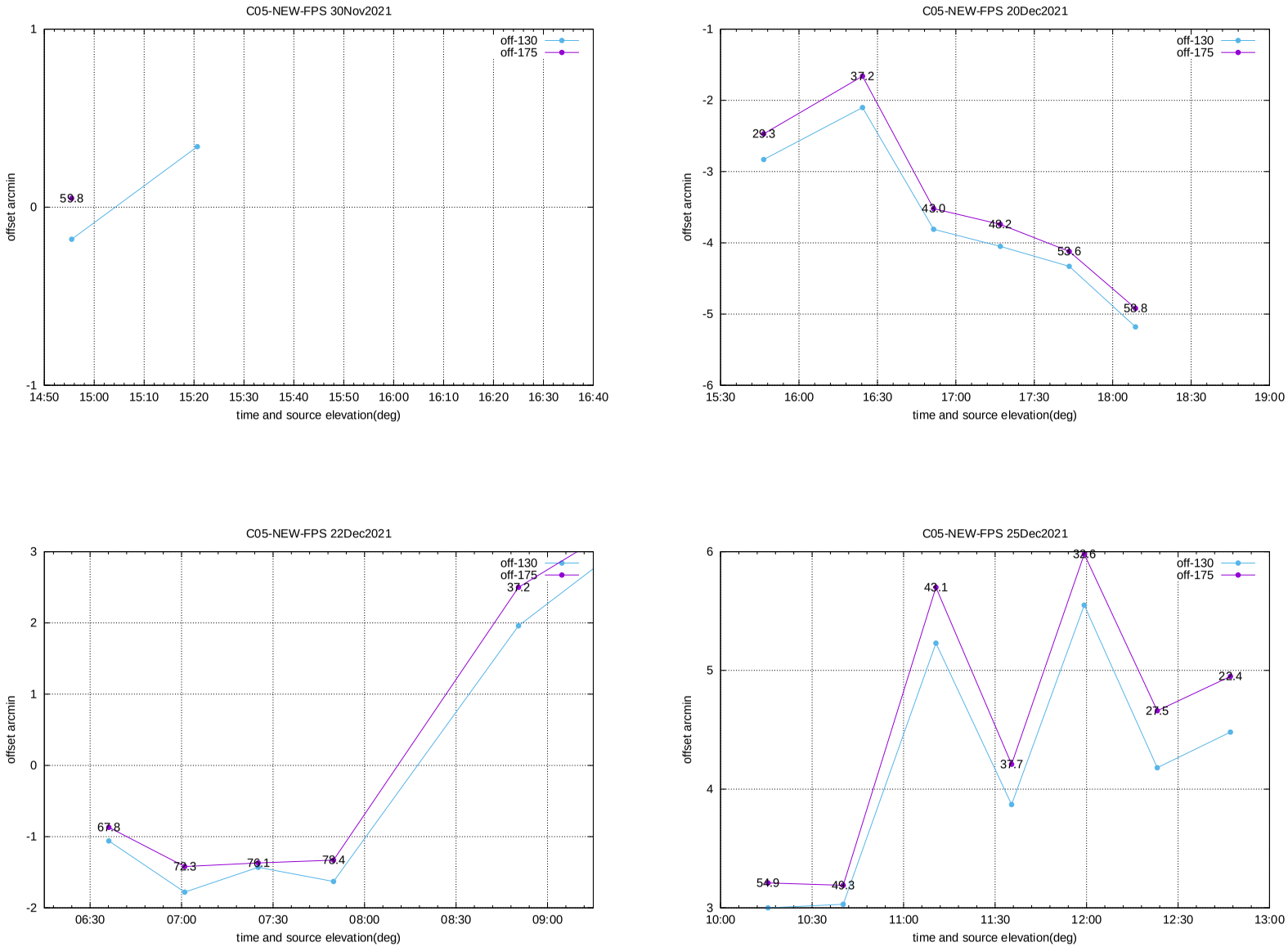

Antenna elevation offset as a function of time and elevation (shown against each points).

Figure 5: Elevation offsets after each `feed-rotation`.

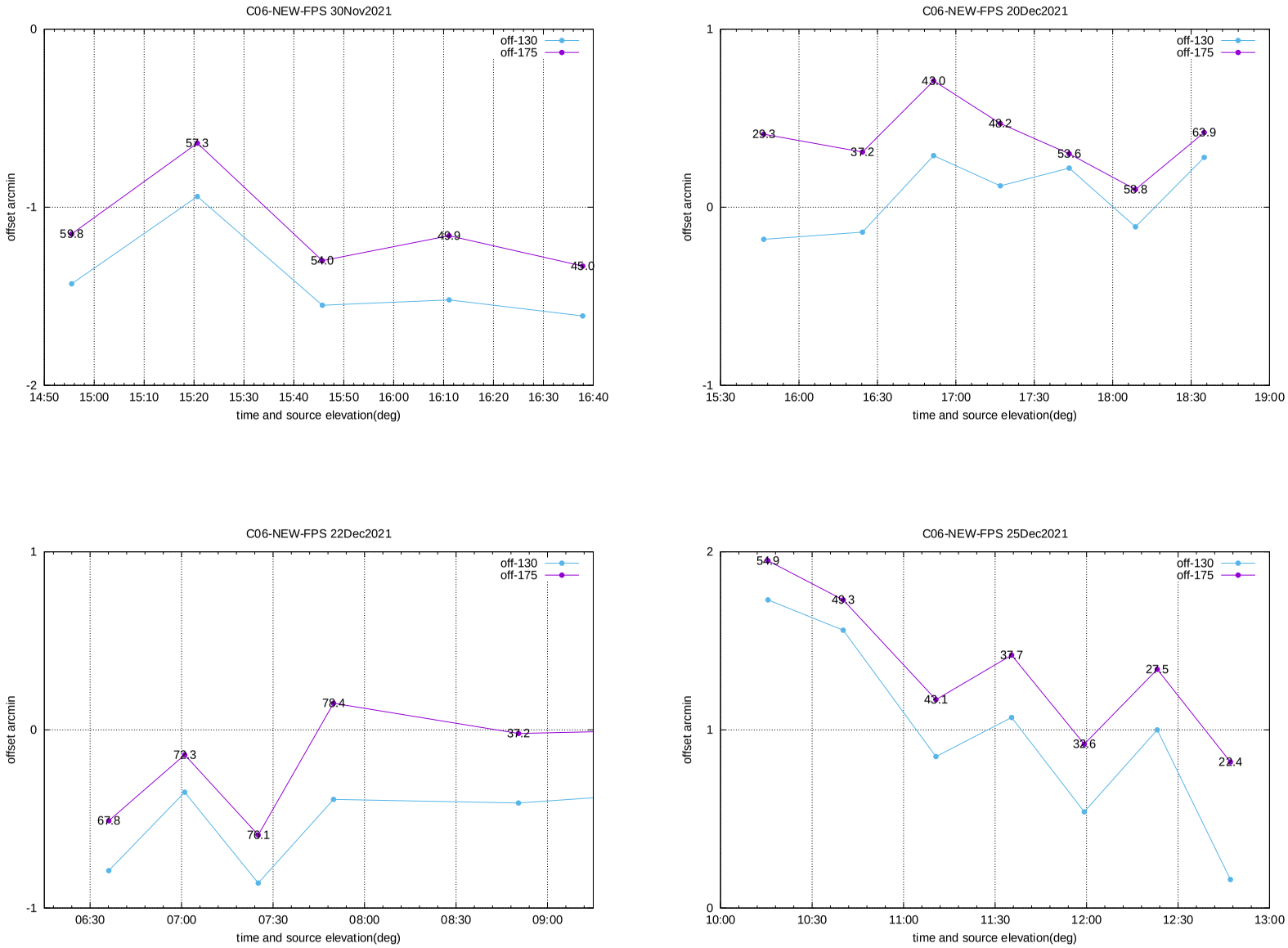

Antenna elevation offset as a function of time and elevation (shown against each points).

Figure 6: Elevation offsets after each `feed-rotation`.

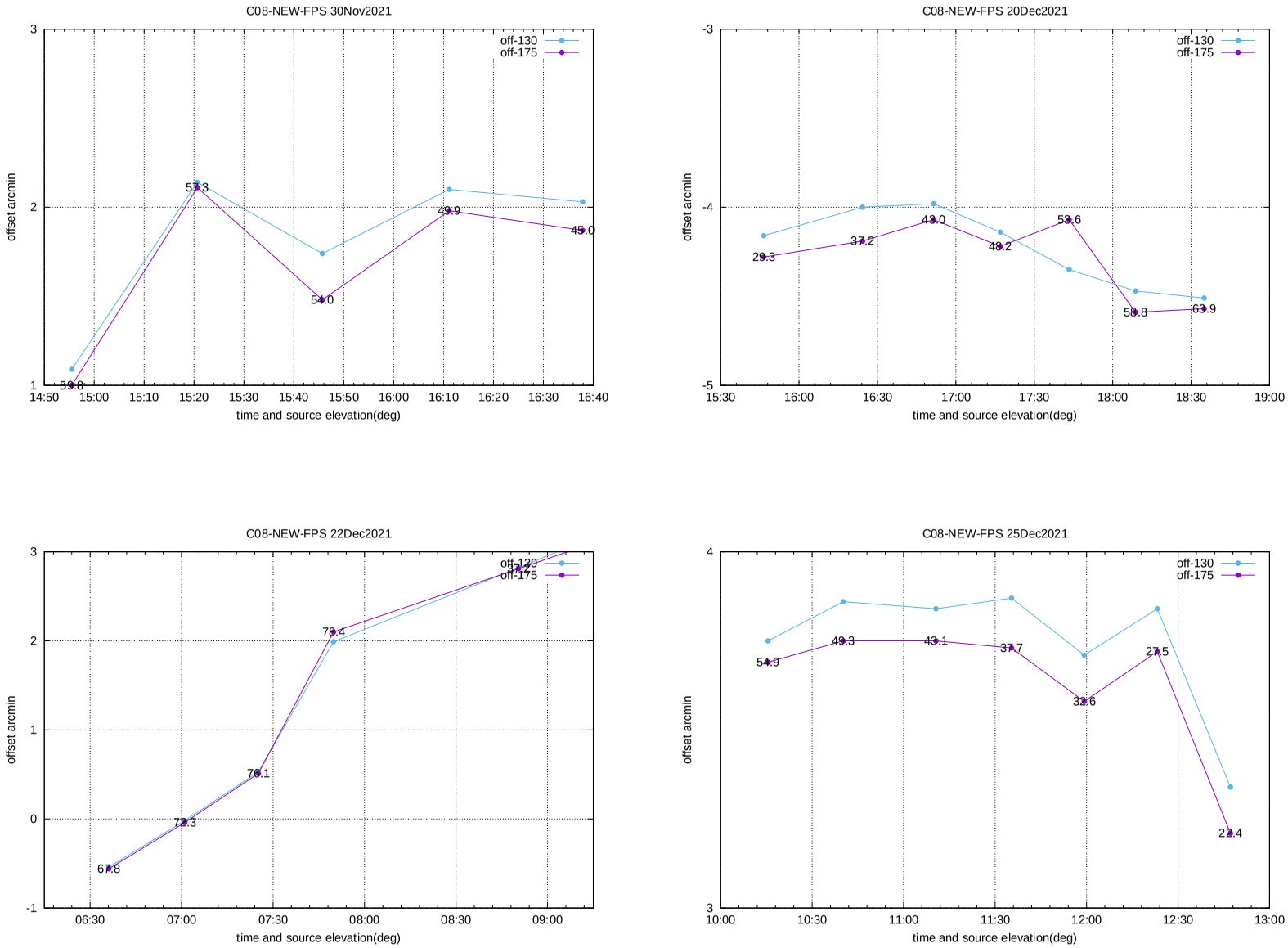

Antenna elevation offset as a function of time and elevation (shown against each points).

Figure 7: Elevation offsets after each `feed-rotation`.

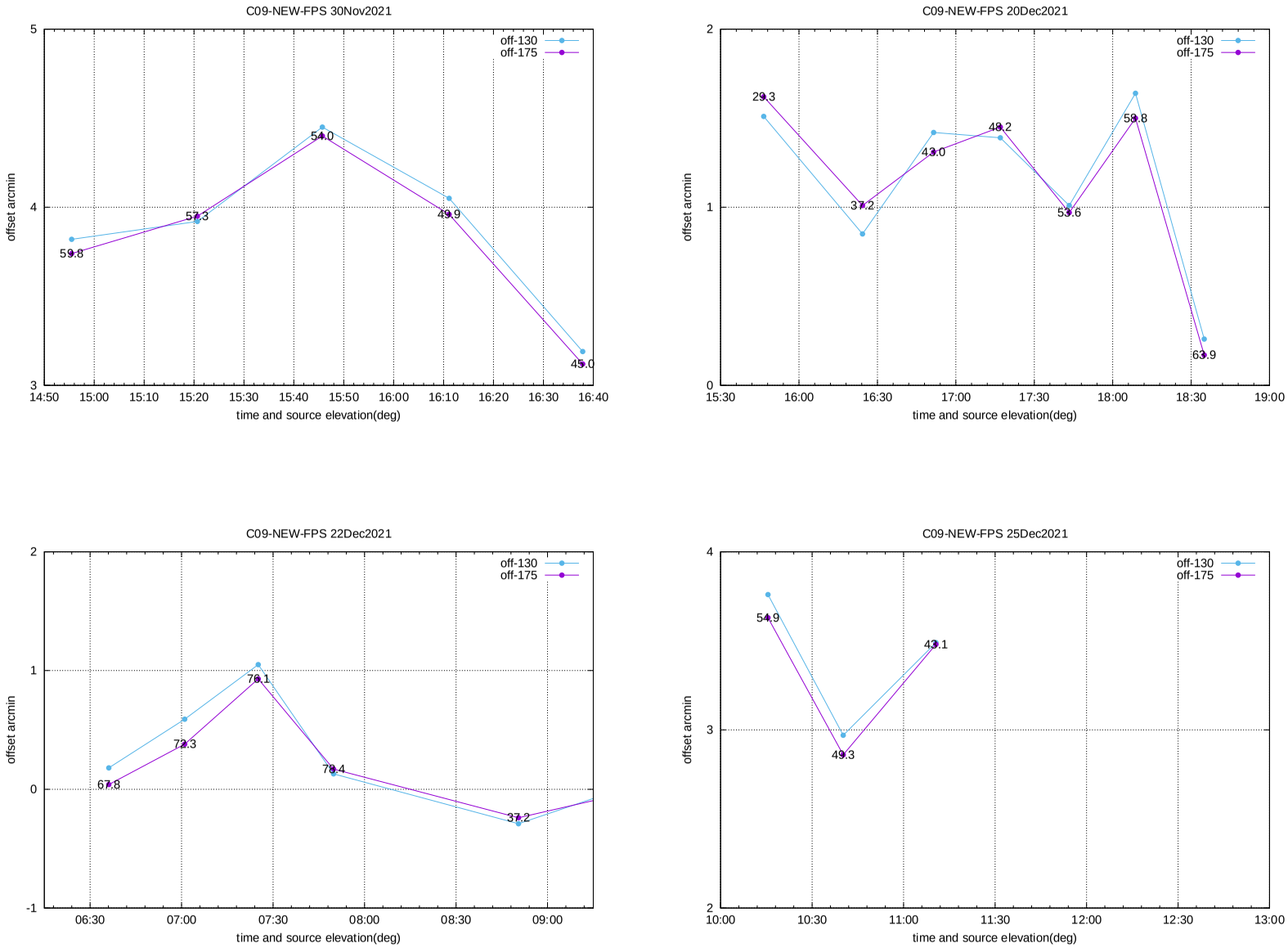

Antenna elevation offset as a function of time and elevation (shown against each points).

Figure 8: Elevation offsets after each `feed-rotation`.

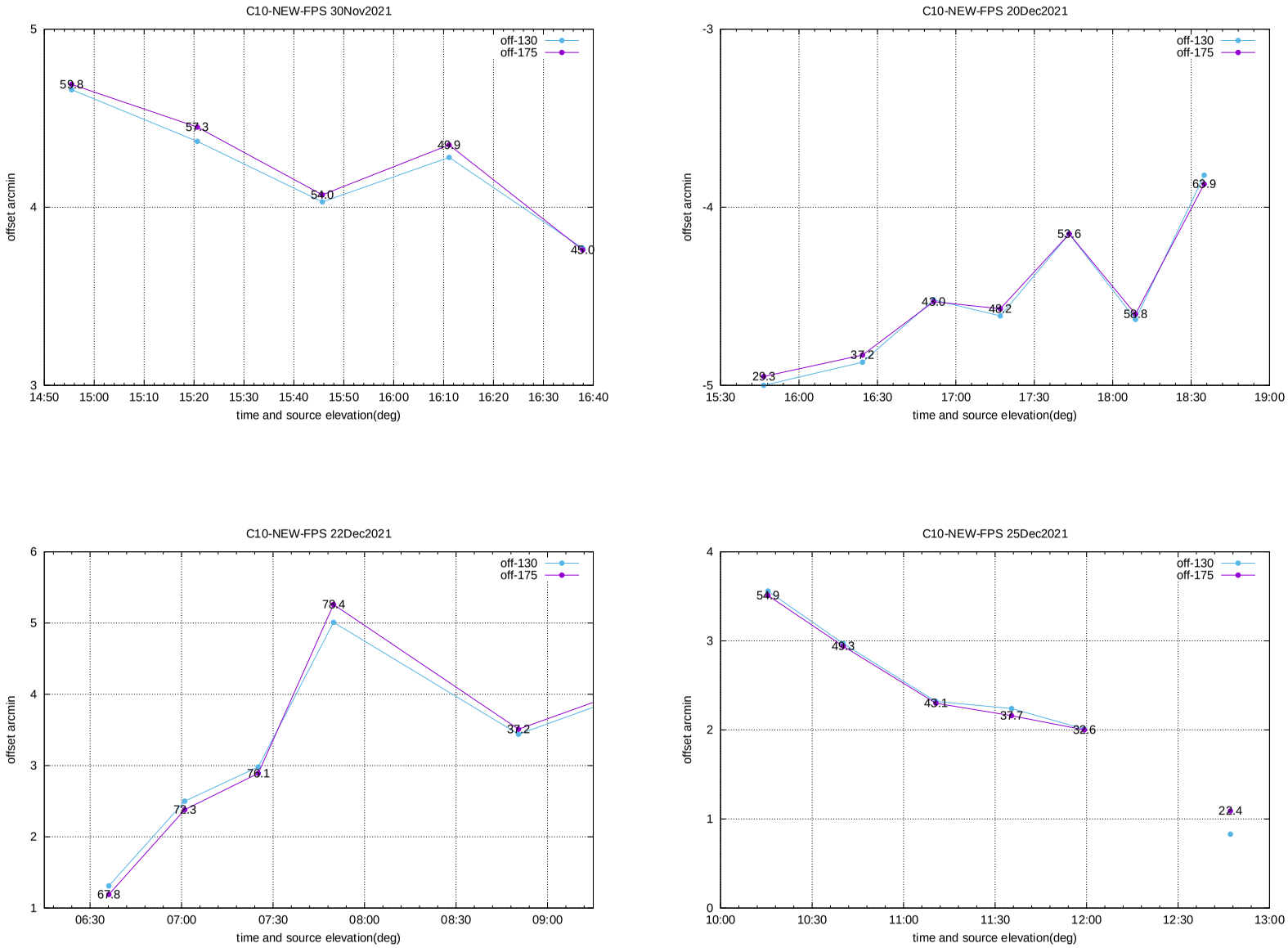

Antenna elevation offset as a function of time and elevation (shown against each points).

Figure 9: Elevation offsets after each `feed-rotation`.

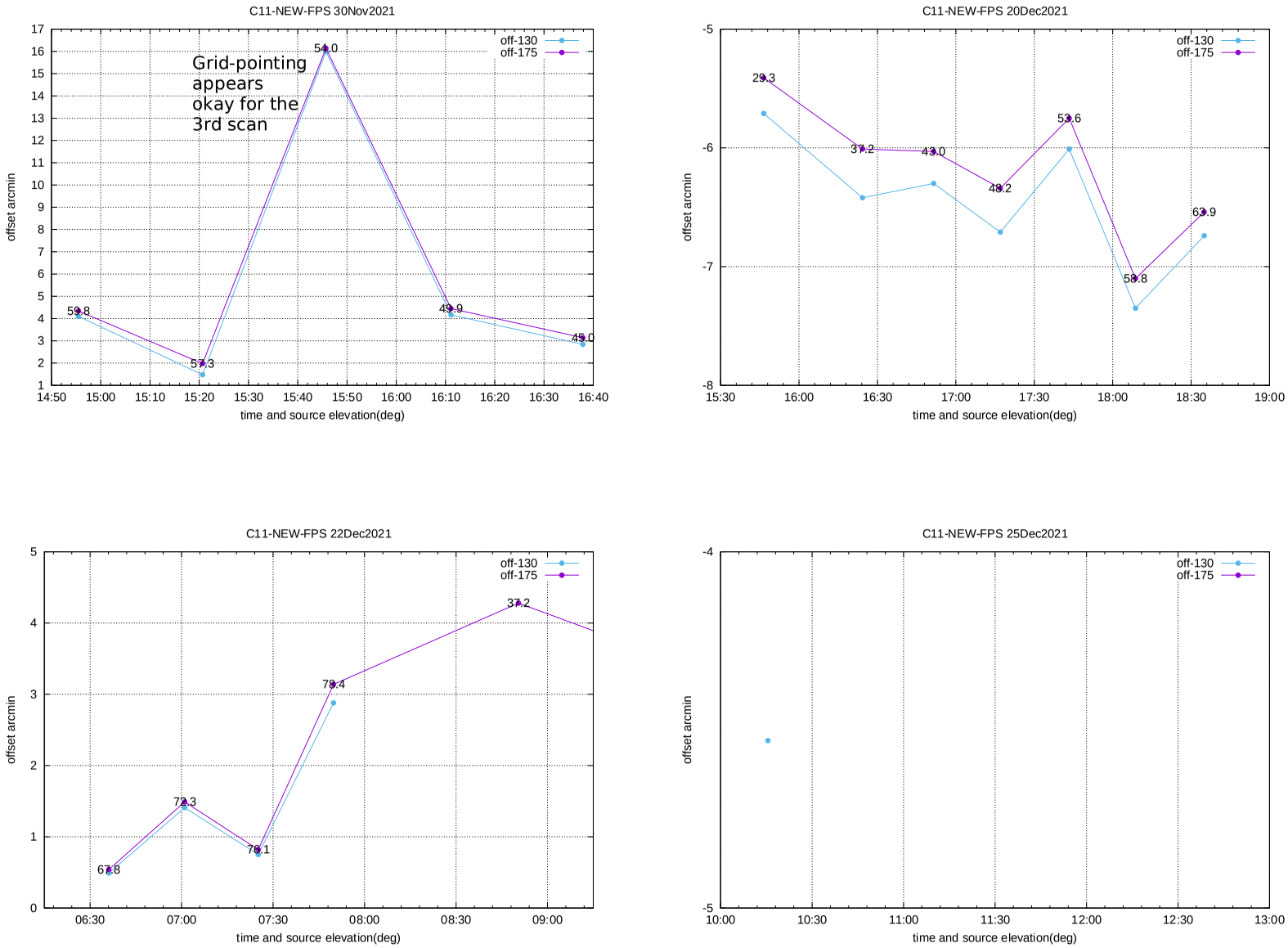

Antenna elevation offset as a function of time and elevation (shown against each points).

Figure 10: Elevation offsets after each `feed-rotation`.

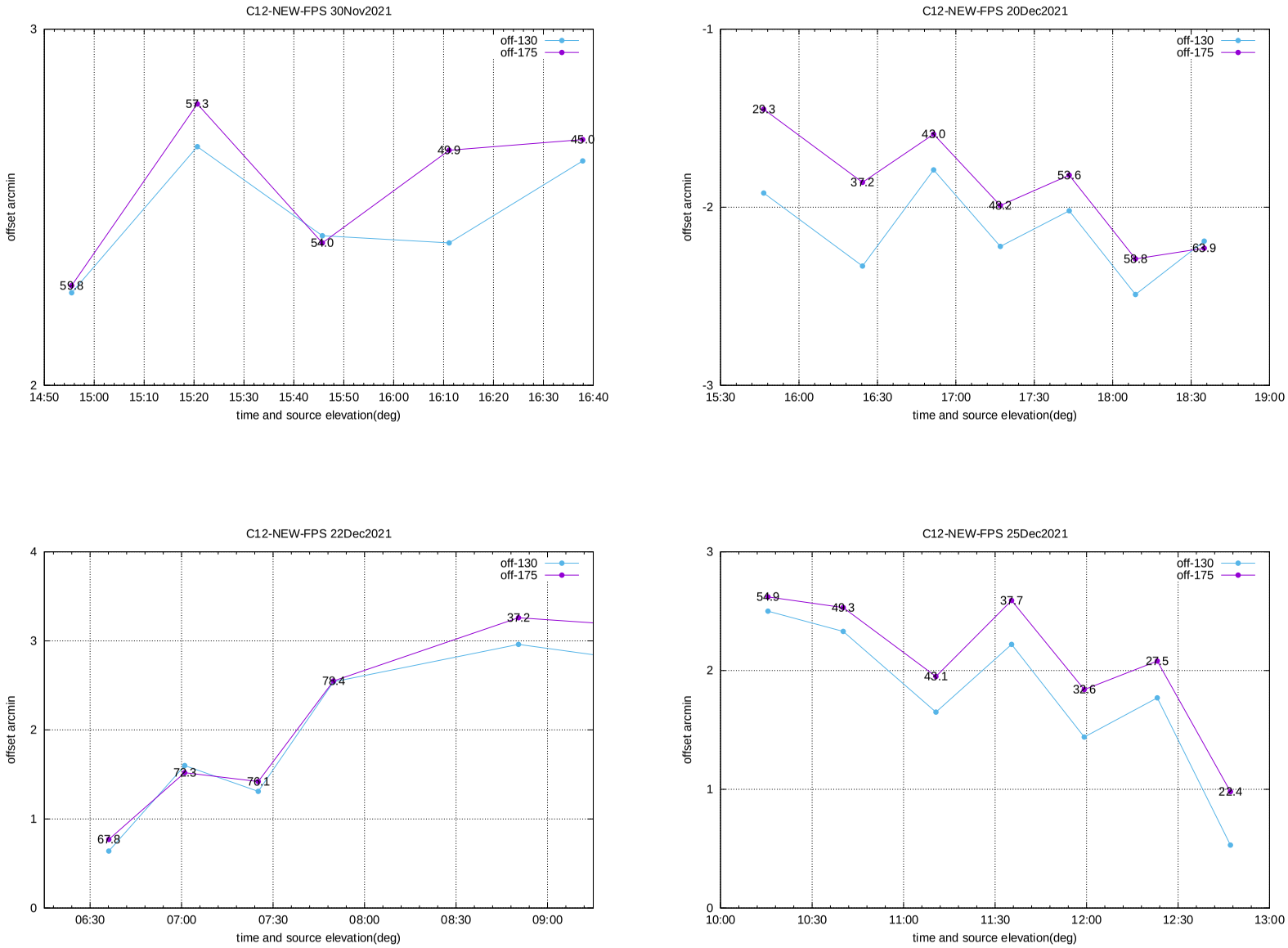

Antenna elevation offset as a function of time and elevation (shown against each points).

Figure 11: Elevation offsets after each `feed-rotation`.

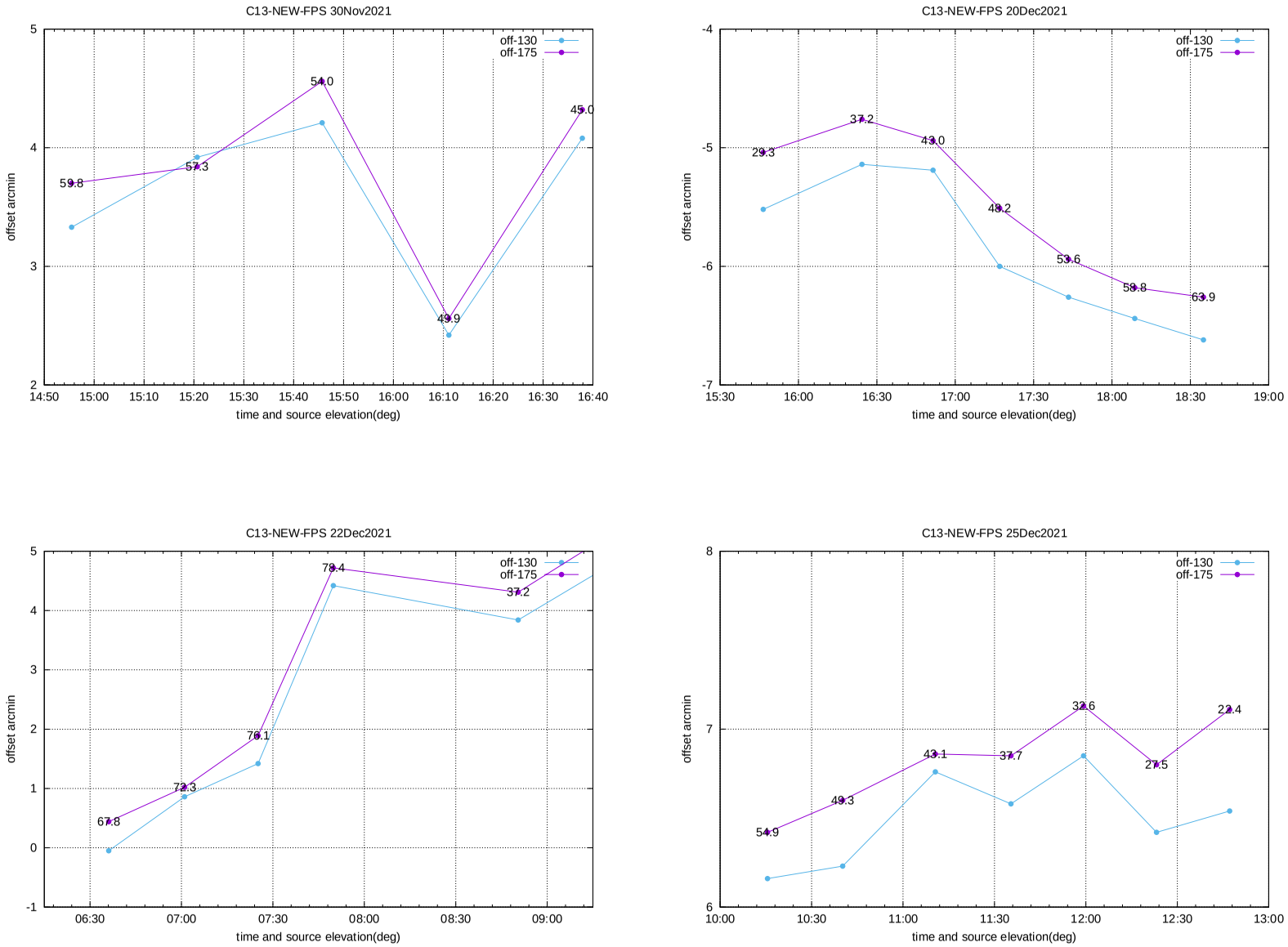

Antenna elevation offset as a function of time and elevation (shown against each points).

Figure 12: Elevation offsets after each `feed-rotation`.

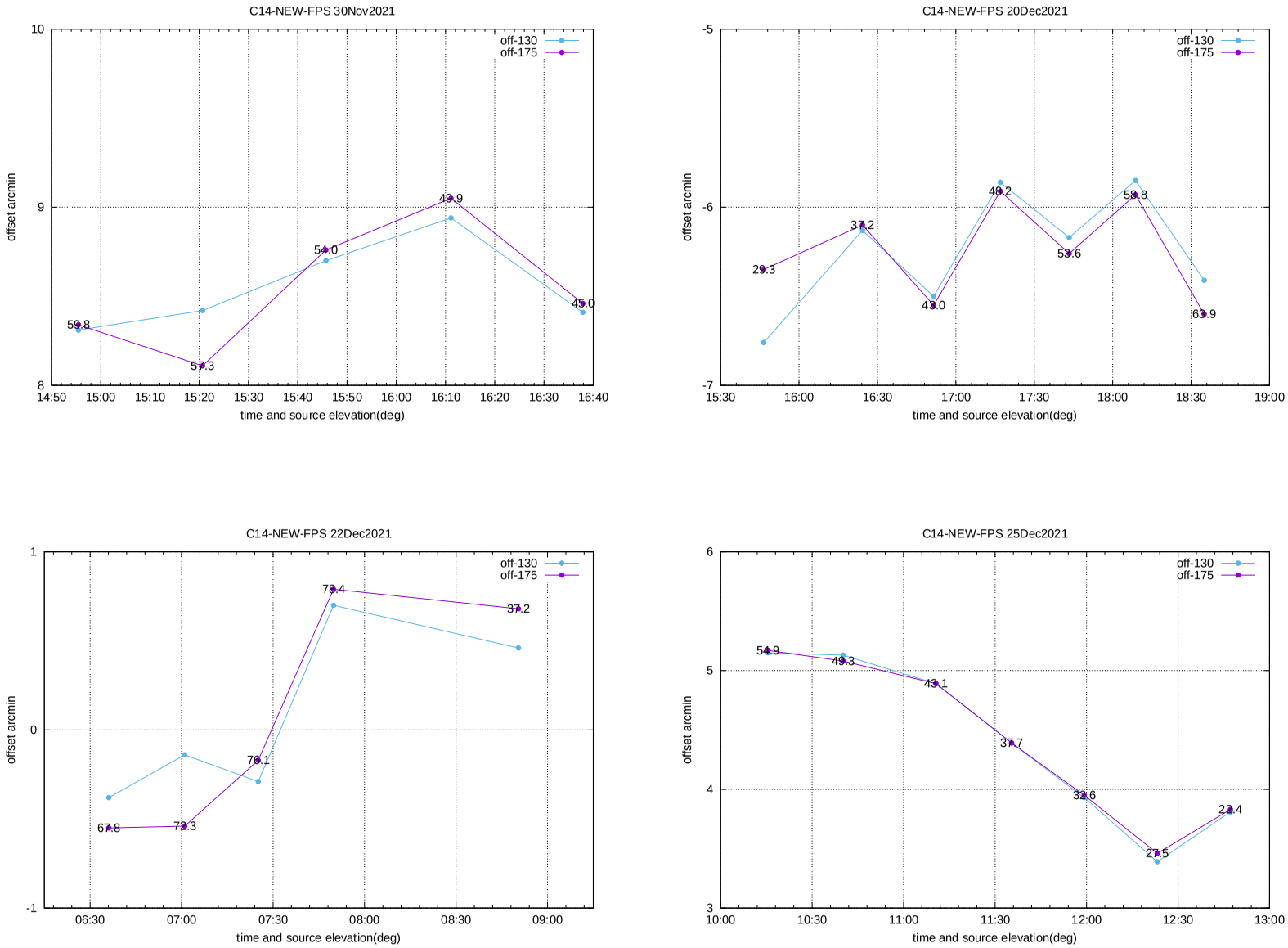

Antenna elevation offset as a function of time and elevation (shown against each points).

Figure 13: Elevation offsets after each `feed-rotation`.

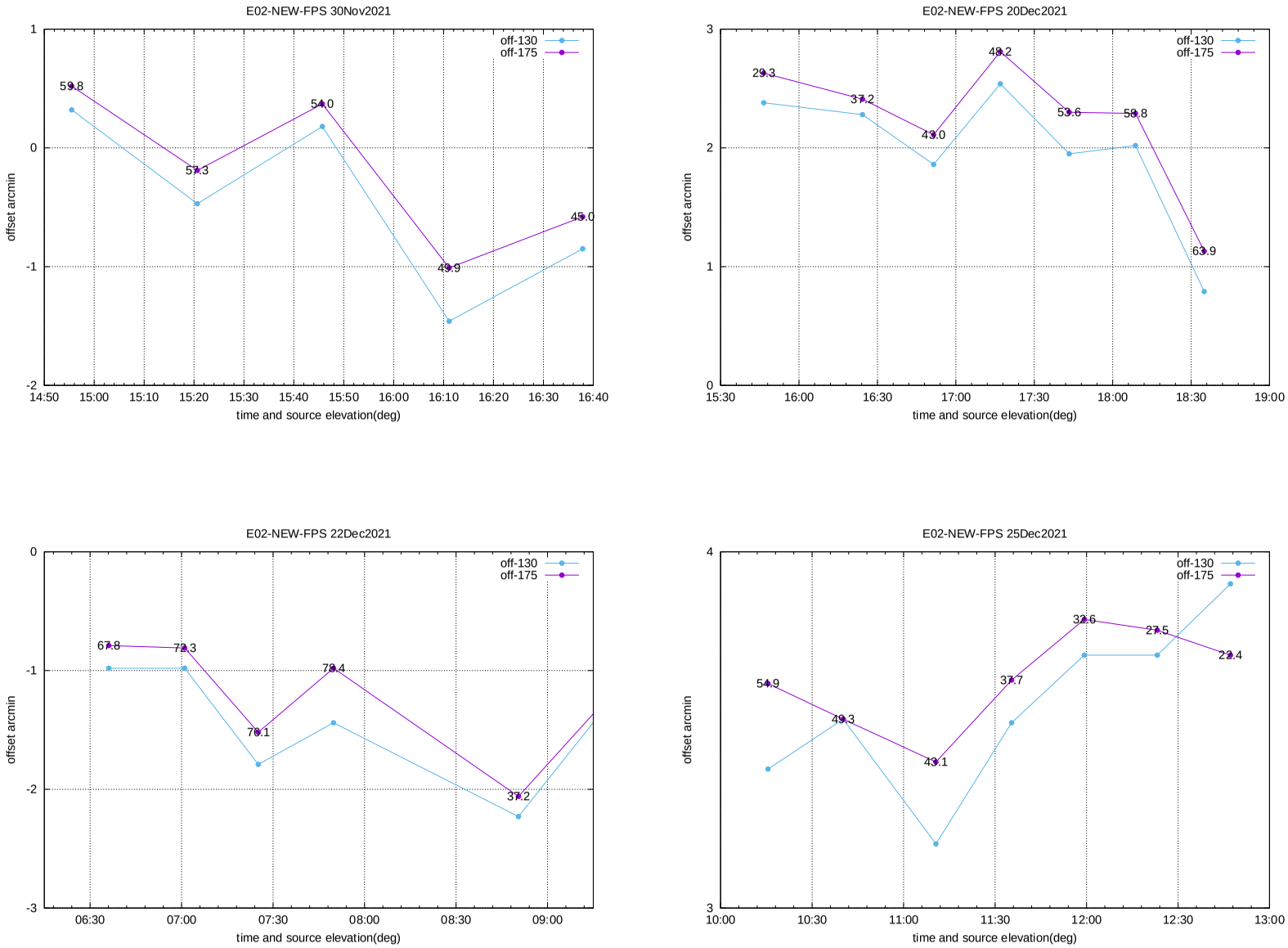

Antenna elevation offset as a function of time and elevation (shown against each points).

Figure 14: Elevation offsets after each `feed-rotation`.

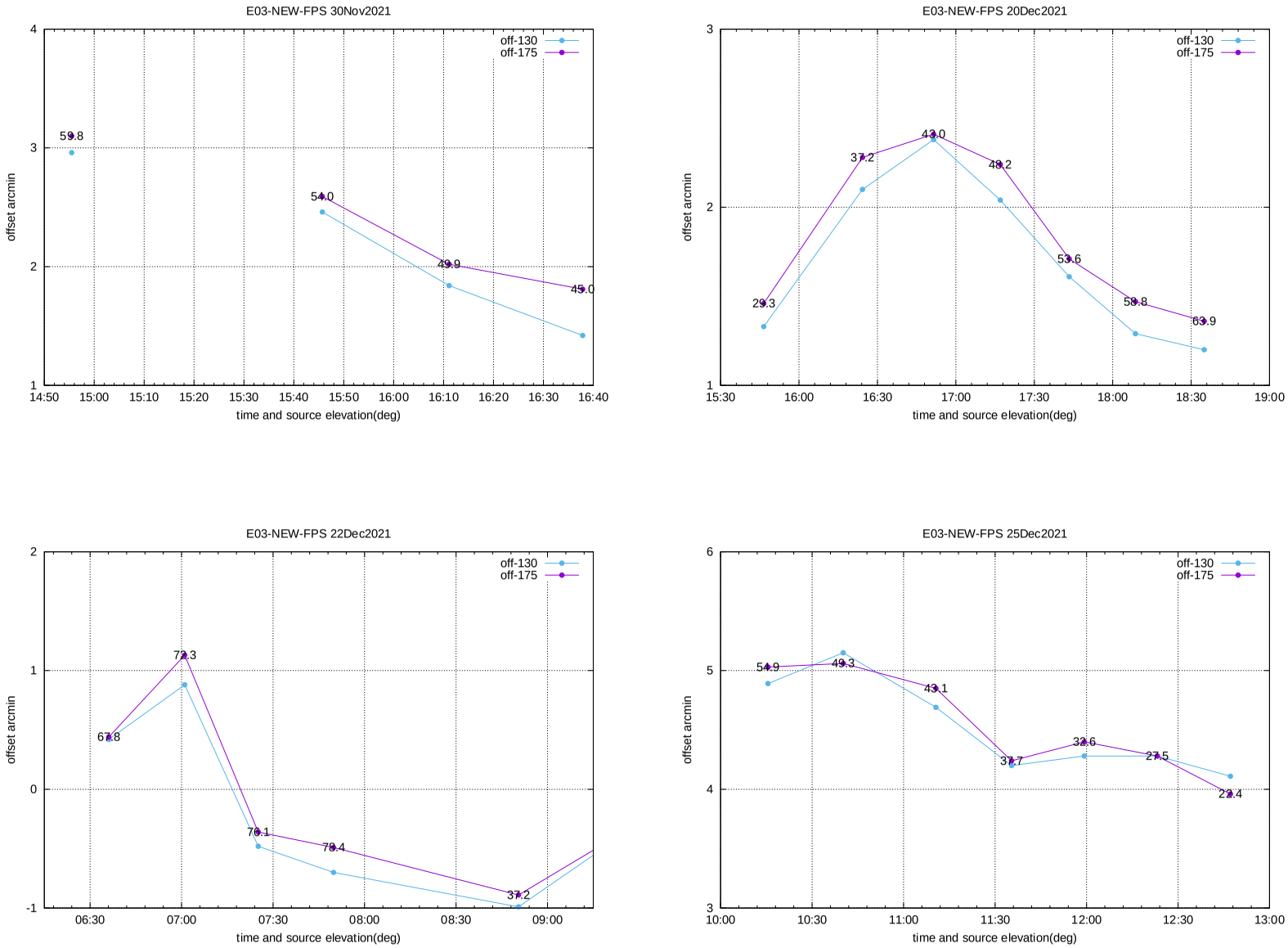

Antenna elevation offset as a function of time and elevation (shown against each points).

Figure 15: Elevation offsets after each `feed-rotation`.

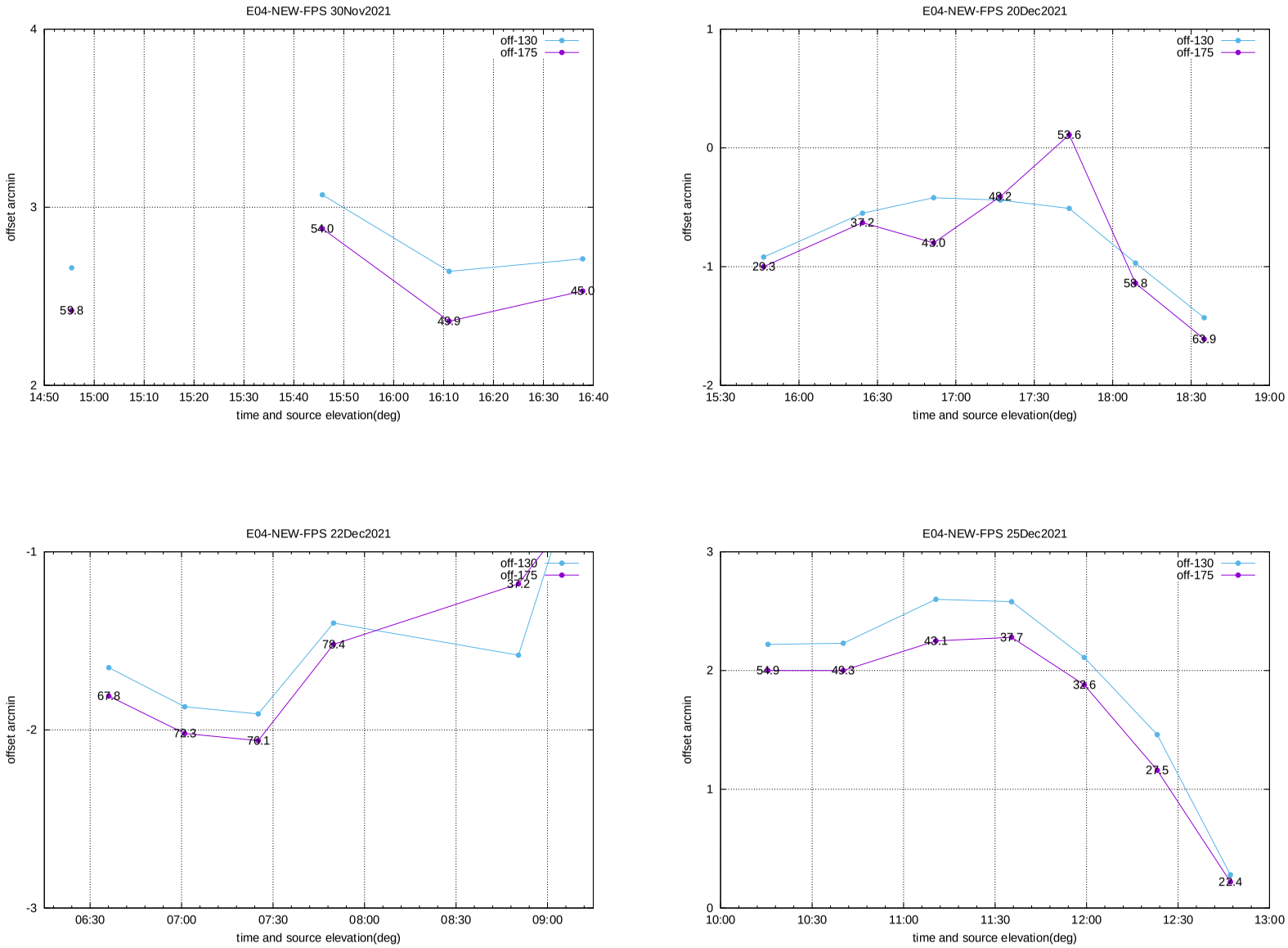

Antenna elevation offset as a function of time and elevation (shown against each points).

Figure 16: Elevation offsets after each `feed-rotation`.

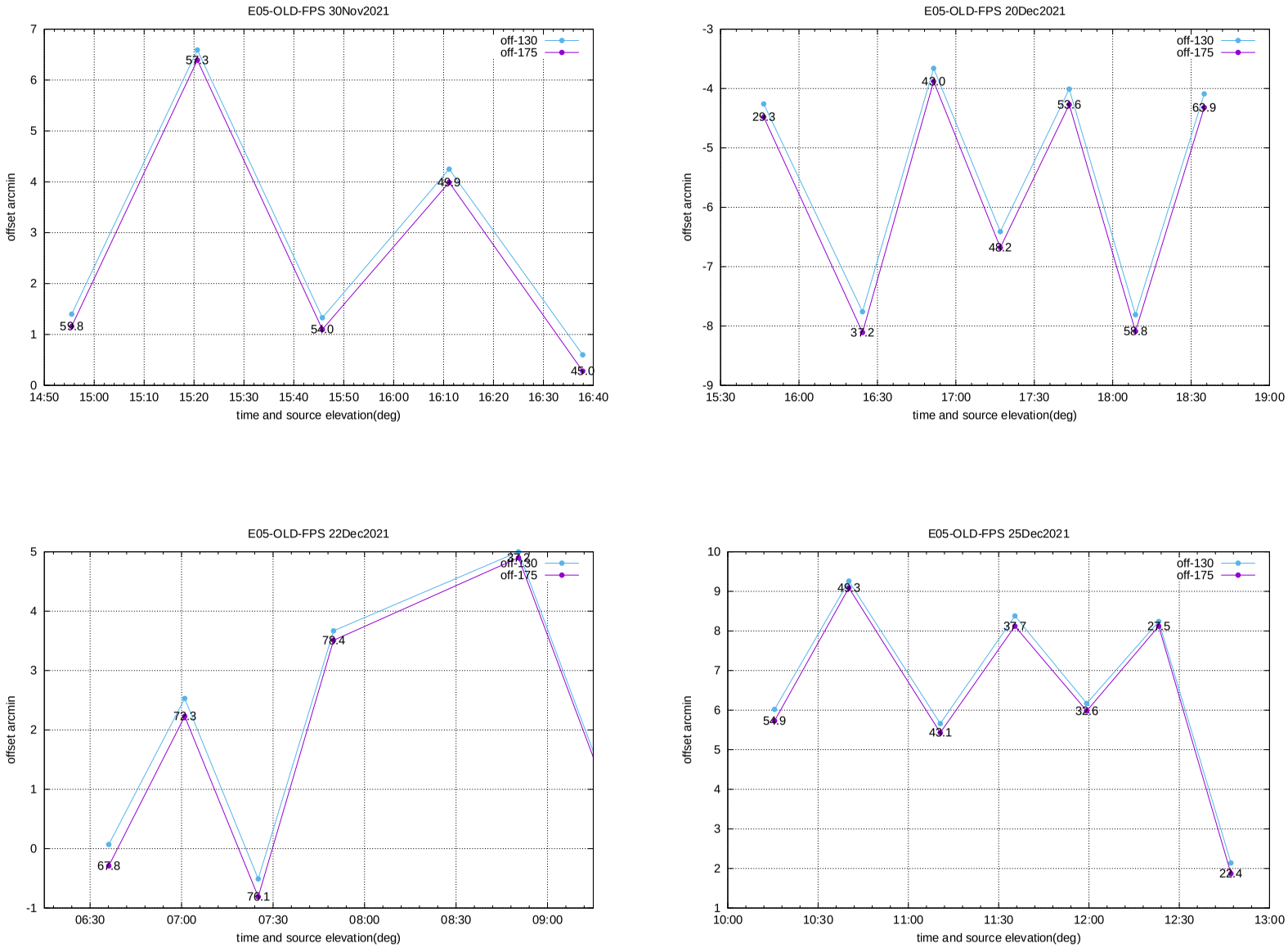

Antenna elevation offset as a function of time and elevation (shown against each points).

Figure 17: Elevation offsets after each `feed-rotation`.

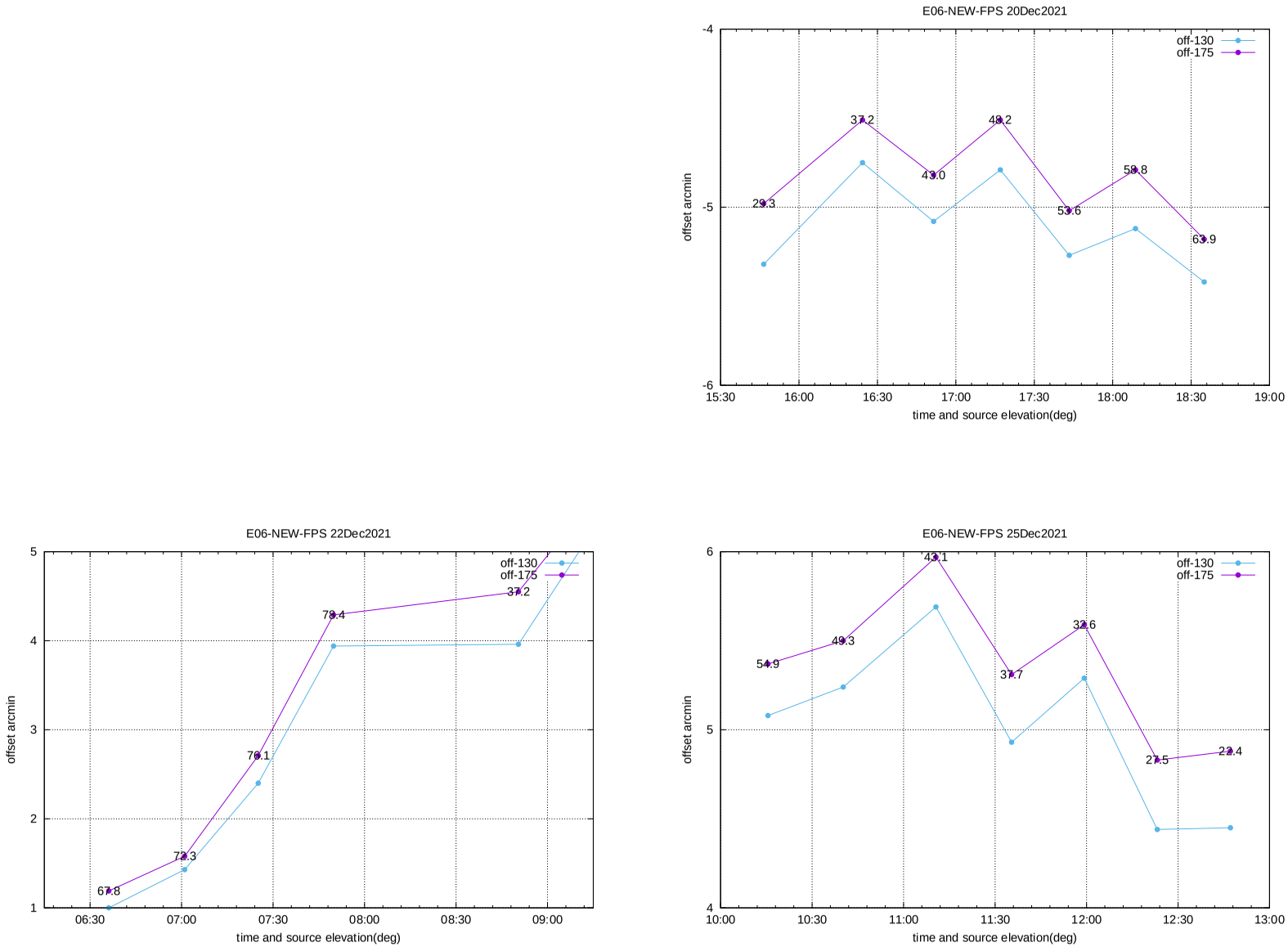

Antenna elevation offset as a function of time and elevation (shown against each points).

Figure 18: Elevation offsets after each `feed-rotation`.

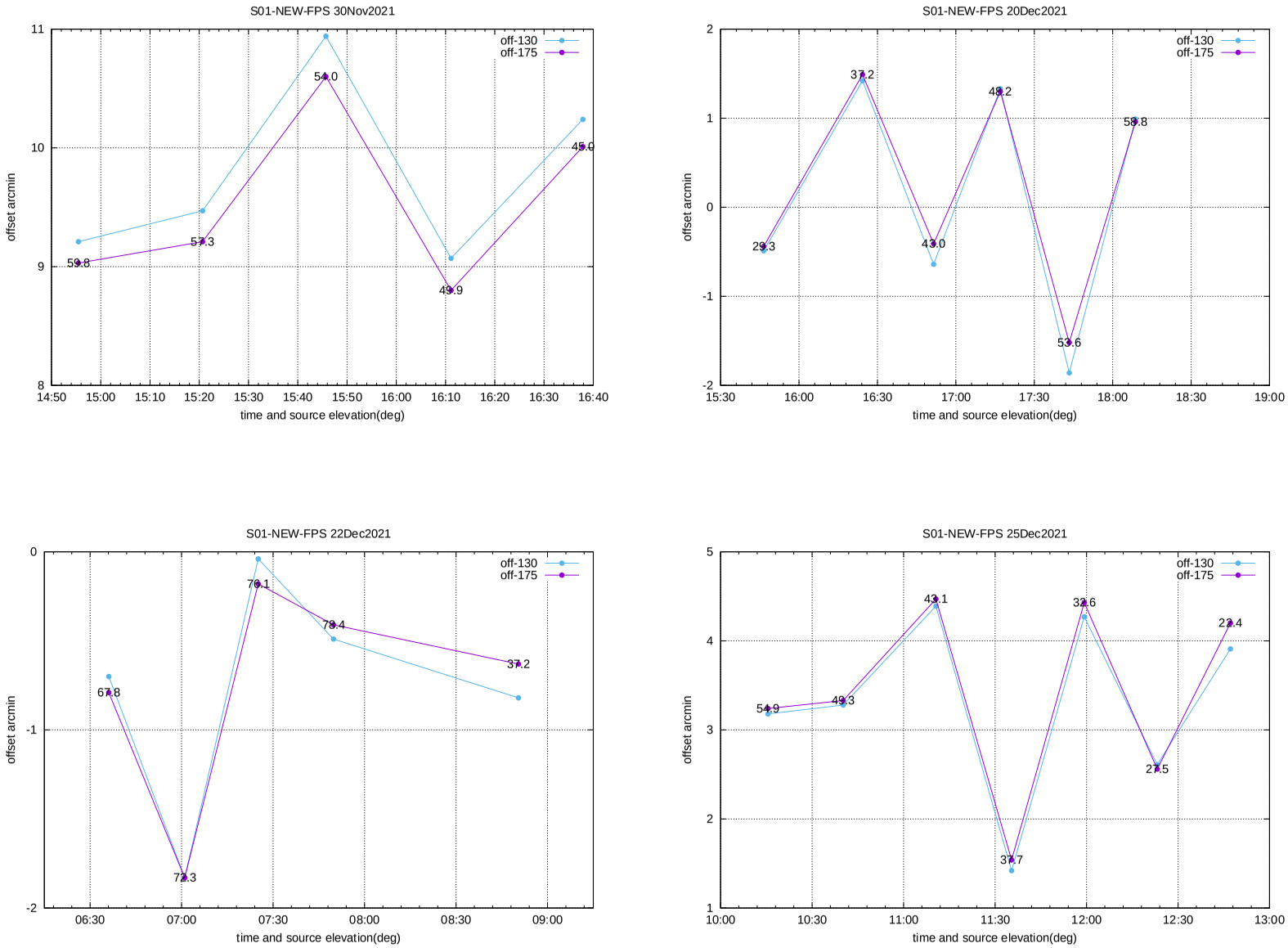

Antenna elevation offset as a function of time and elevation (shown against each points).

Figure 19: Elevation offsets after each `feed-rotation`.

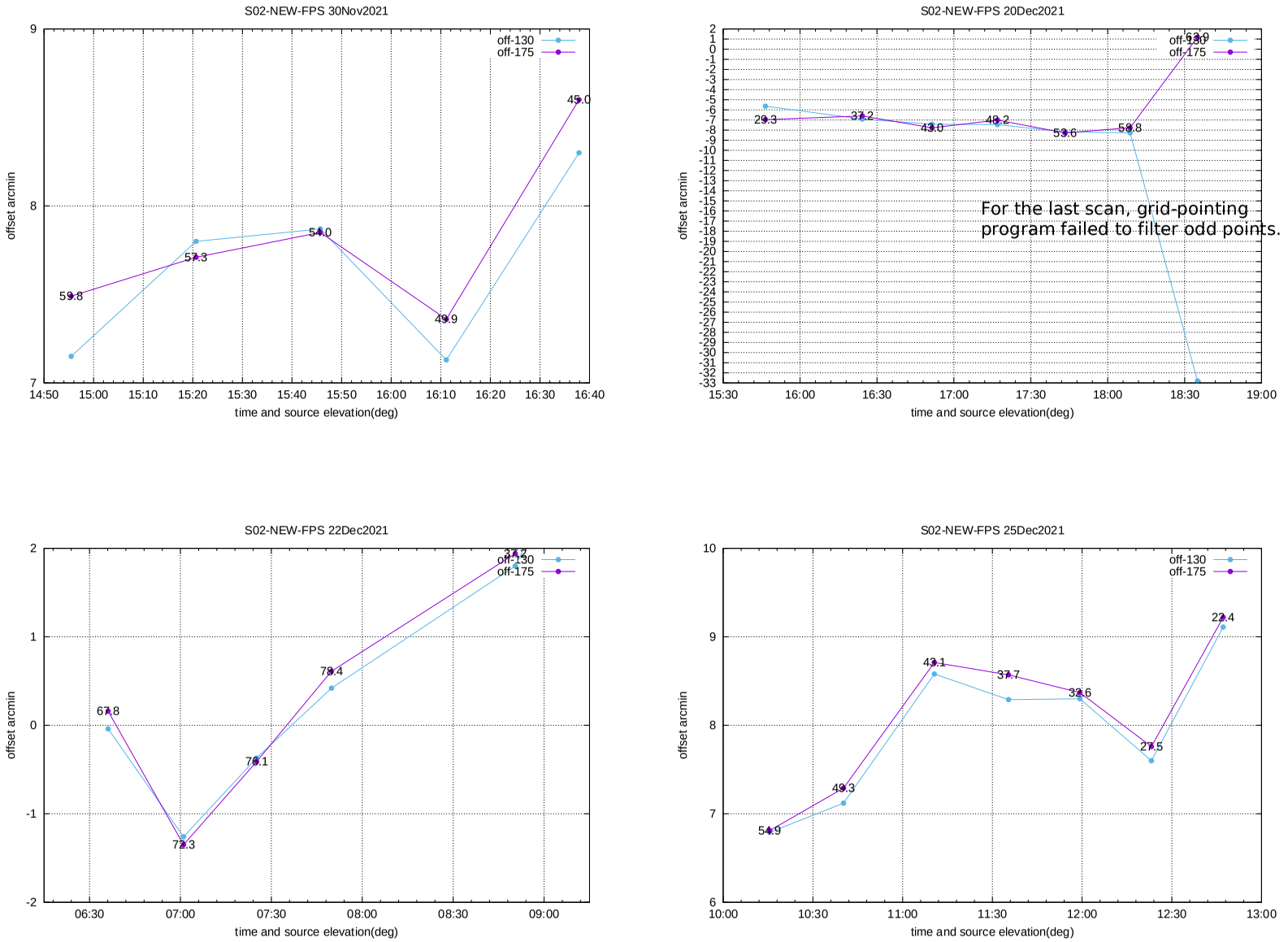

Antenna elevation offset as a function of time and elevation (shown against each points).

Figure 20: Elevation offsets after each `feed-rotation`.

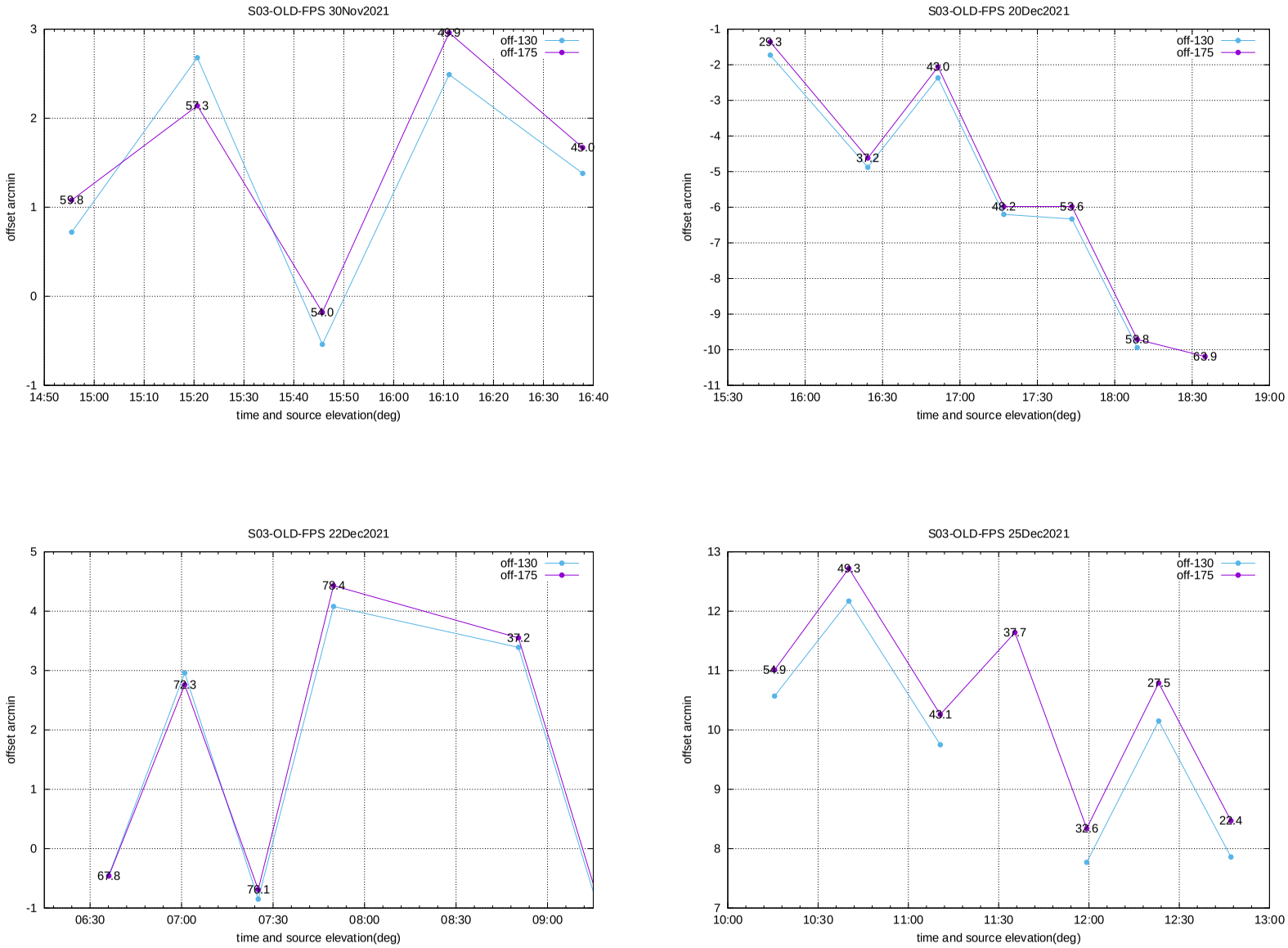

Antenna elevation offset as a function of time and elevation (shown against each points).

Figure 21: Elevation offsets after each `feed-rotation`.

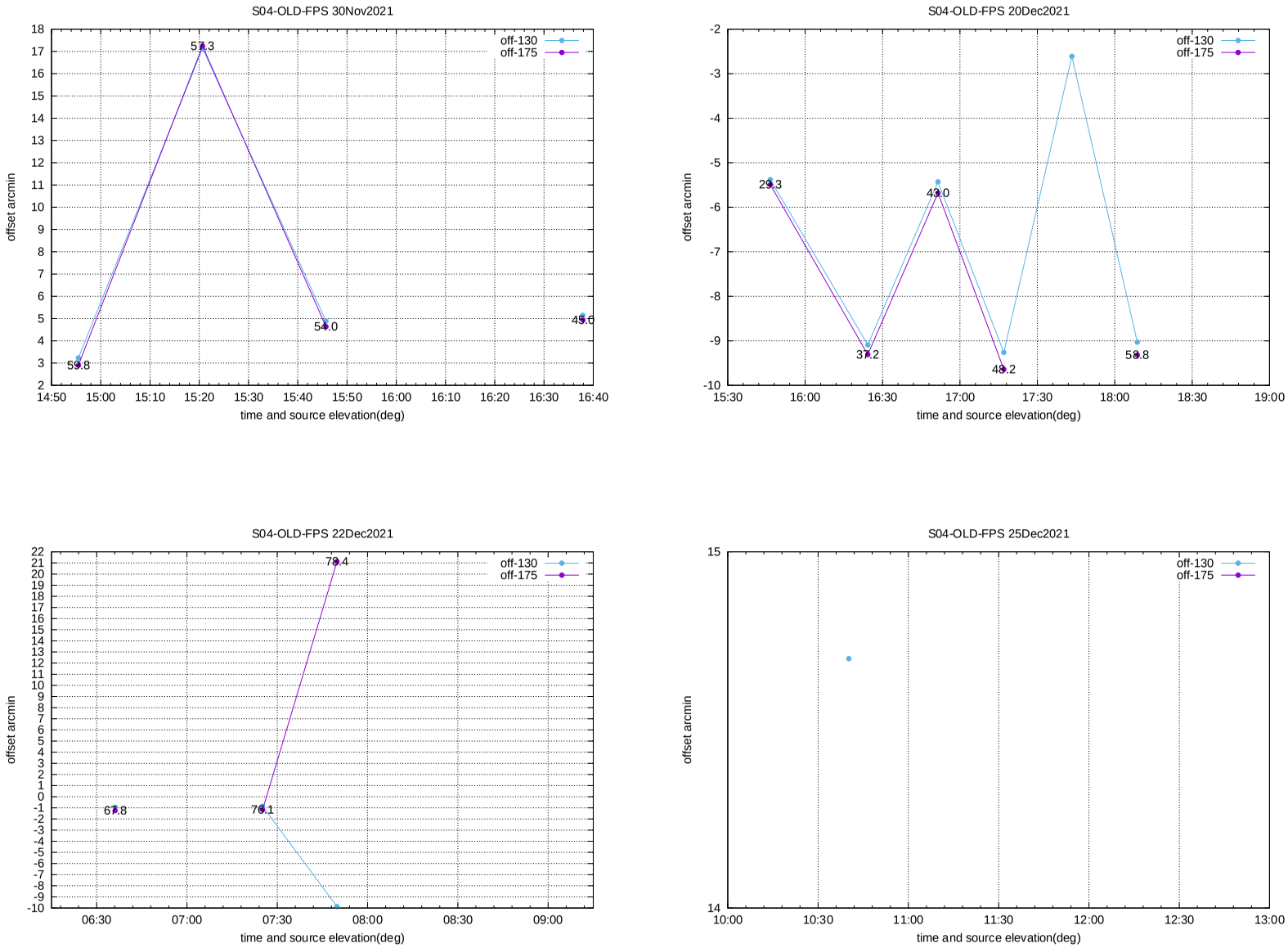

Antenna elevation offset as a function of time and elevation (shown against each points).

Figure 22: Elevation offsets after each `feed-rotation`.

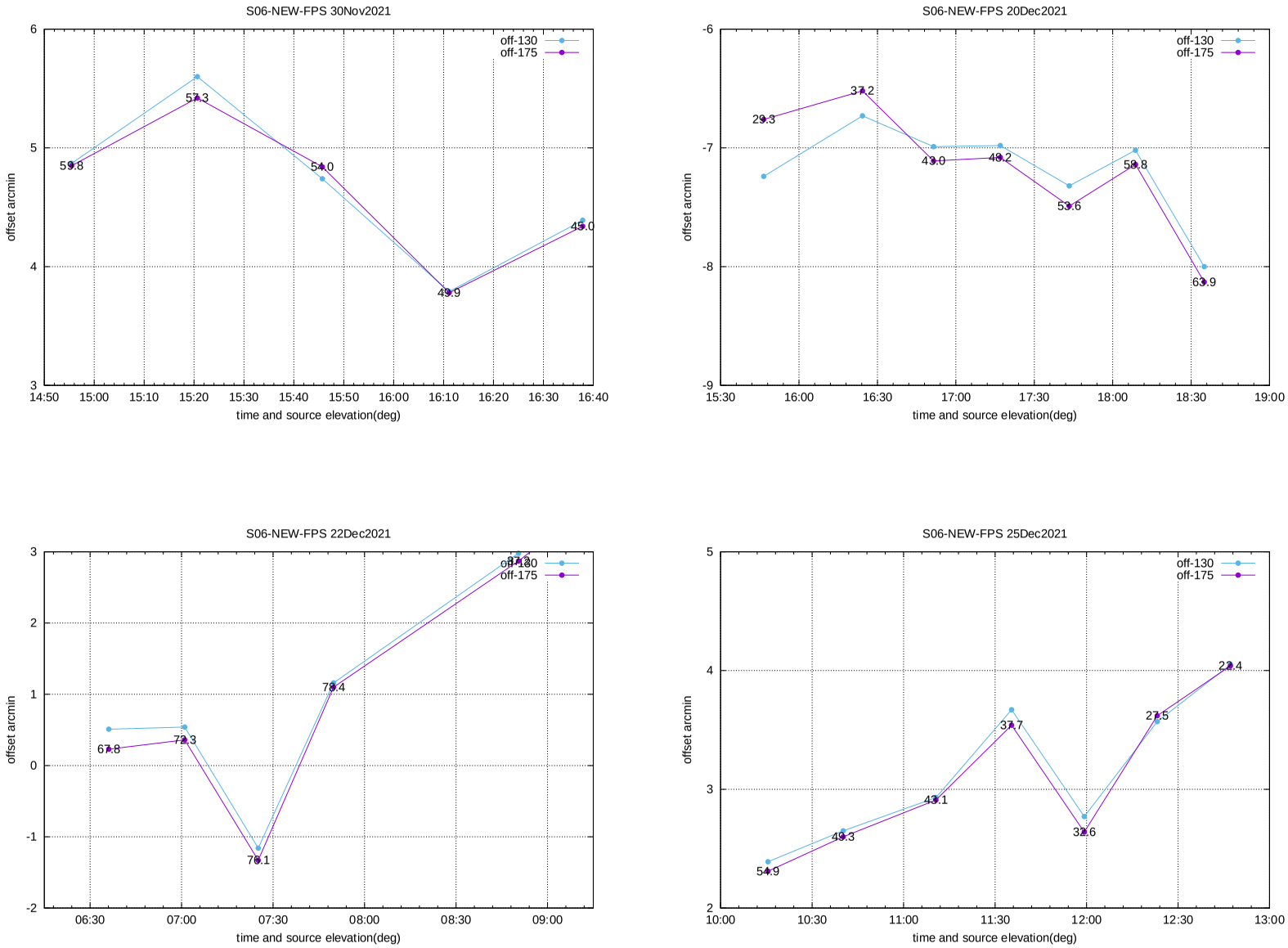

Antenna elevation offset as a function of time and elevation (shown against each points).

Figure 23: Elevation offsets after each `feed-rotation`.

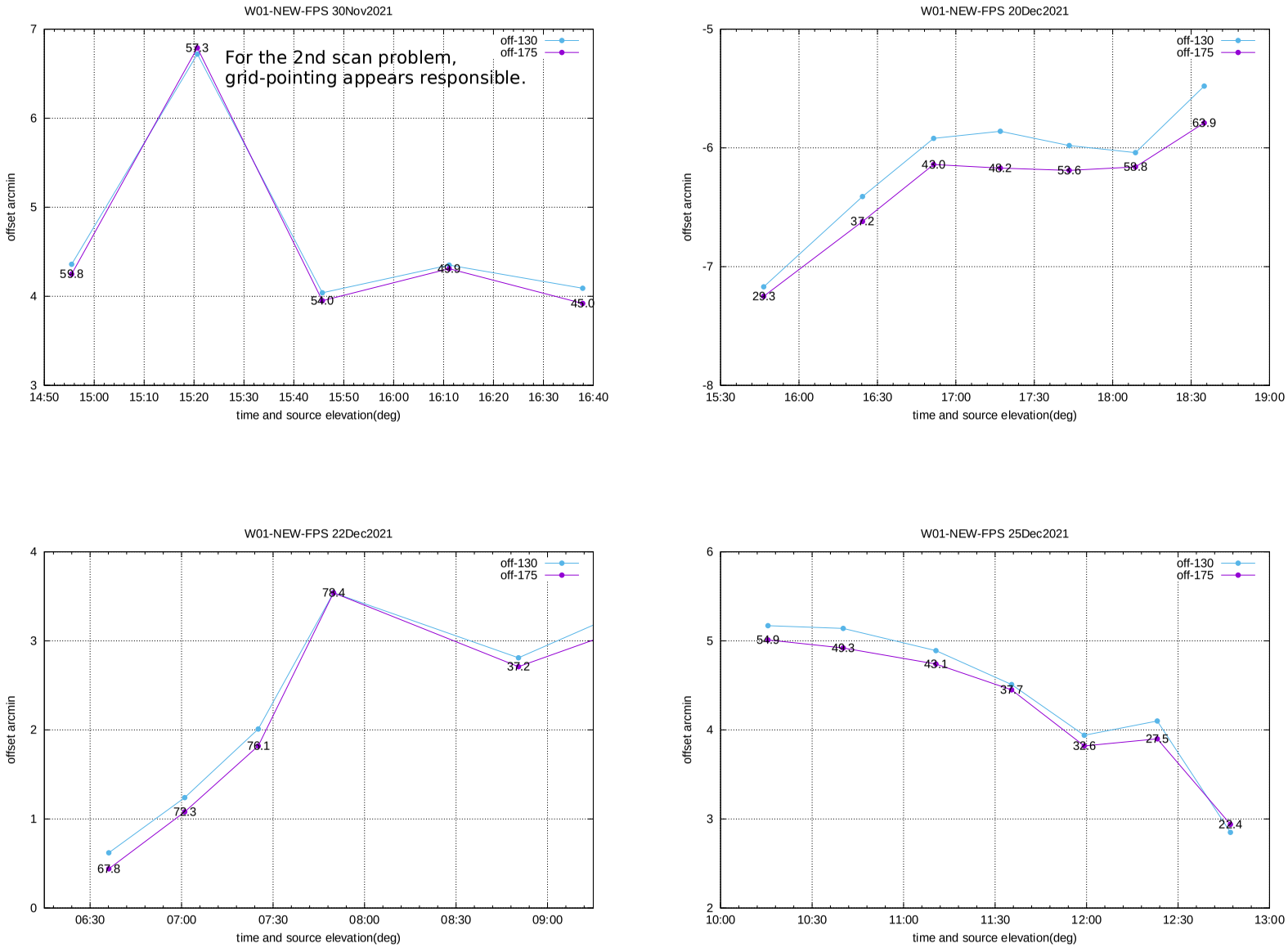

Antenna elevation offset as a function of time and elevation (shown against each points).

Figure 24: Elevation offsets after each `feed-rotation`.

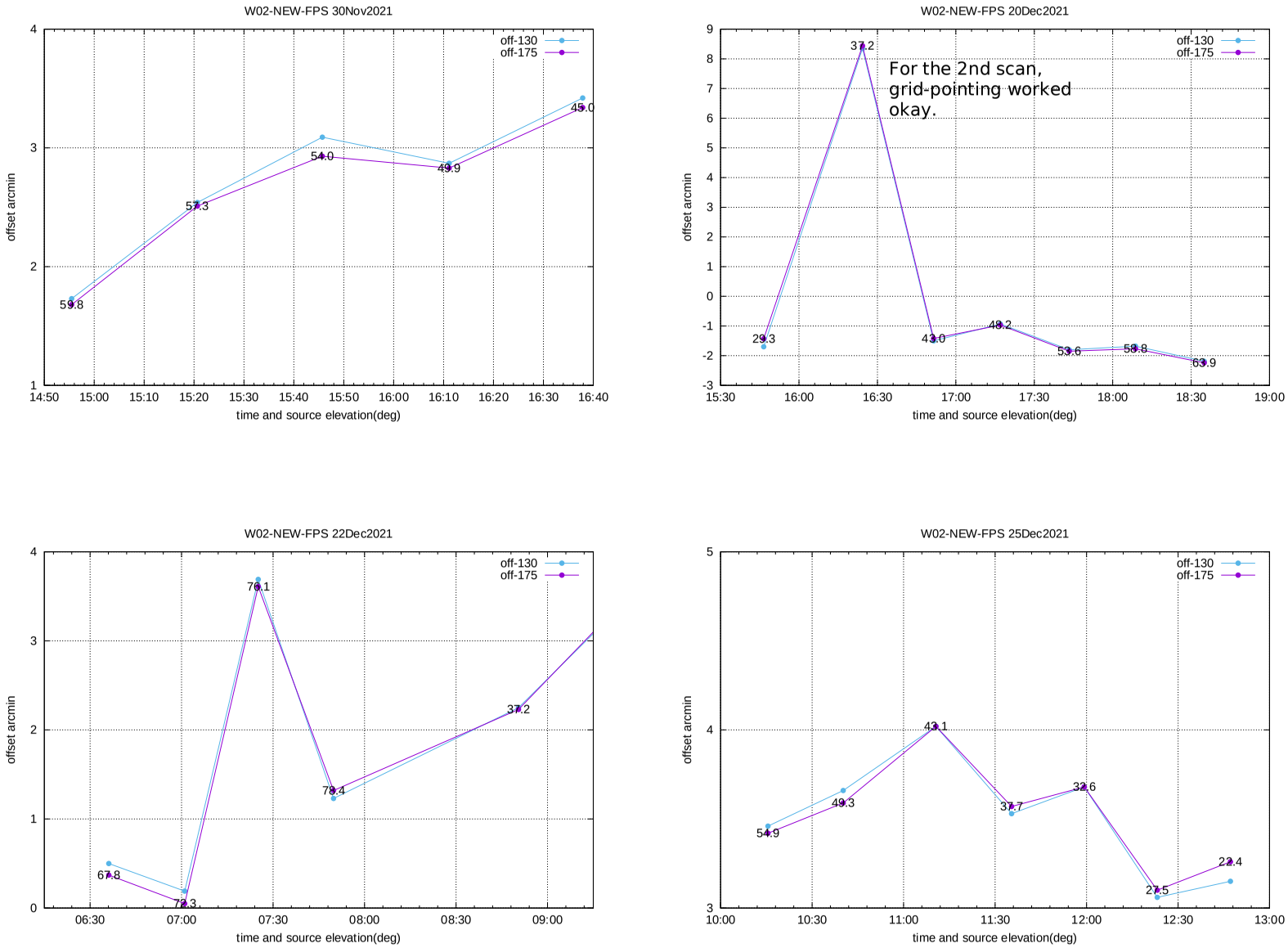

Antenna elevation offset as a function of time and elevation (shown against each points).

Figure 25: Elevation offsets after each `feed-rotation`.

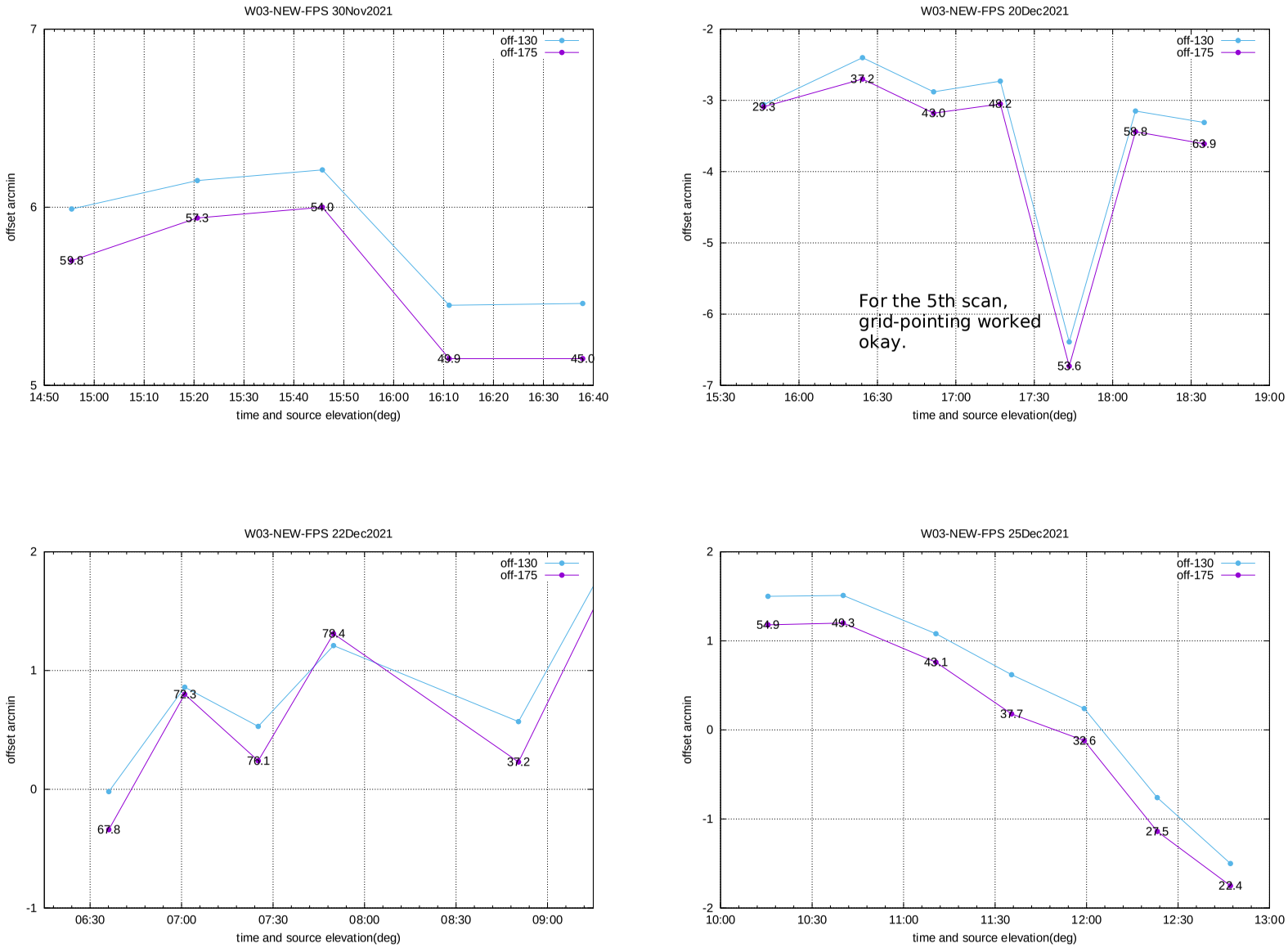

Antenna elevation offset as a function of time and elevation (shown against each points).

Figure 26: Elevation offsets after each `feed-rotation`.

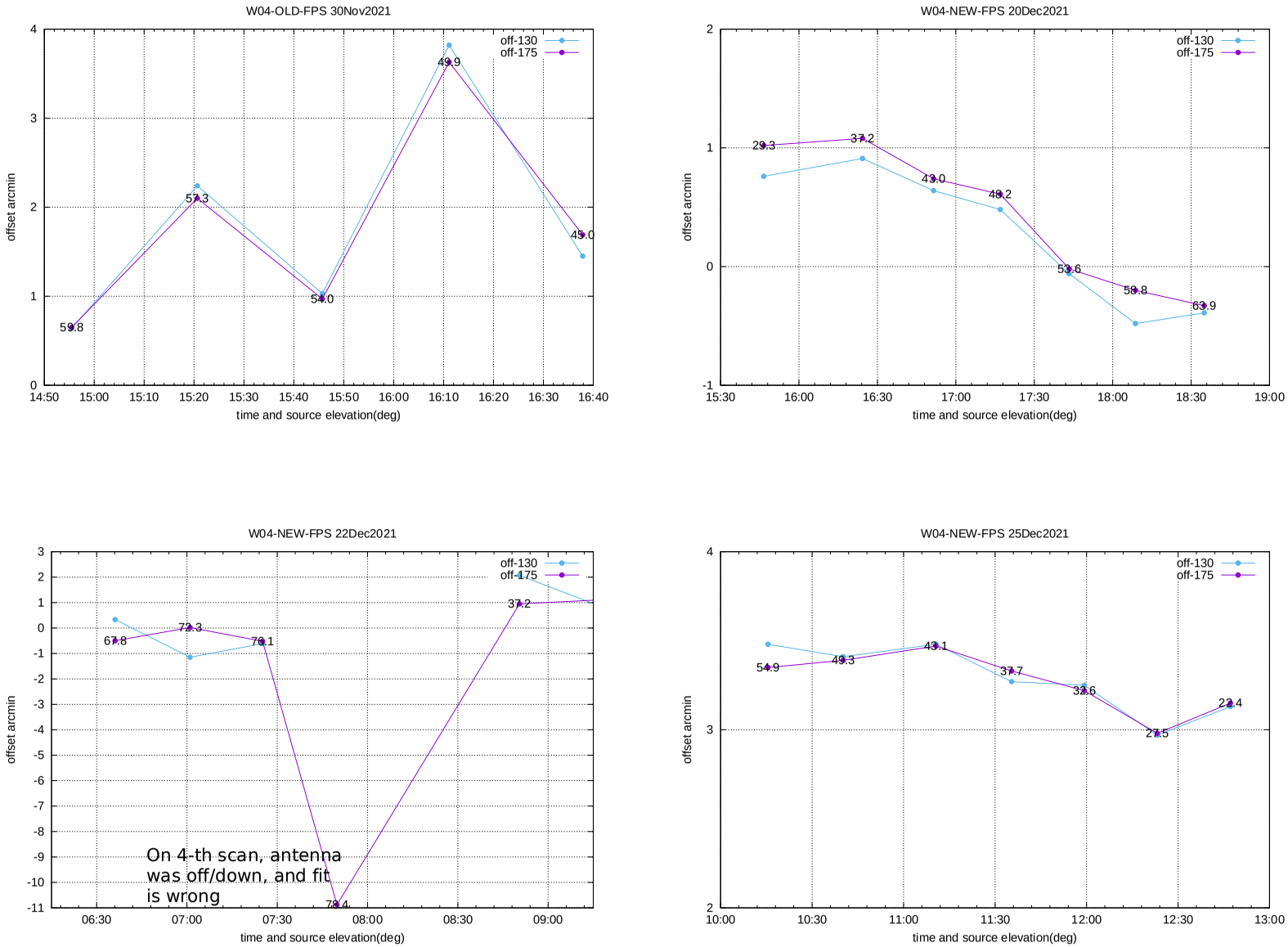

Antenna elevation offset as a function of time and elevation (shown against each points).

Figure 27: Elevation offsets after each `feed-rotation`.

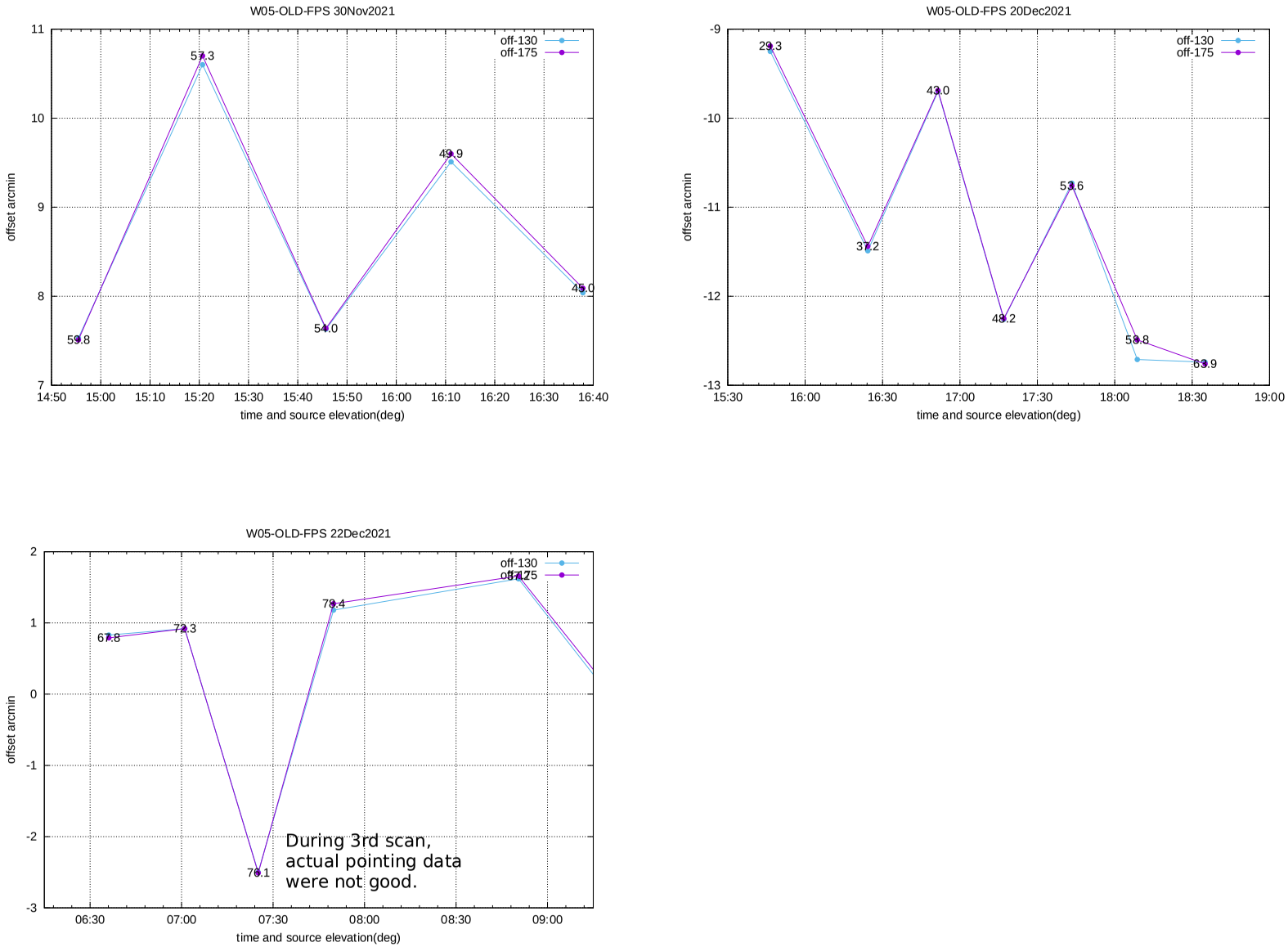

Antenna elevation offset as a function of time and elevation (shown against each points).

Figure 28: Elevation offsets after each `feed-rotation`.

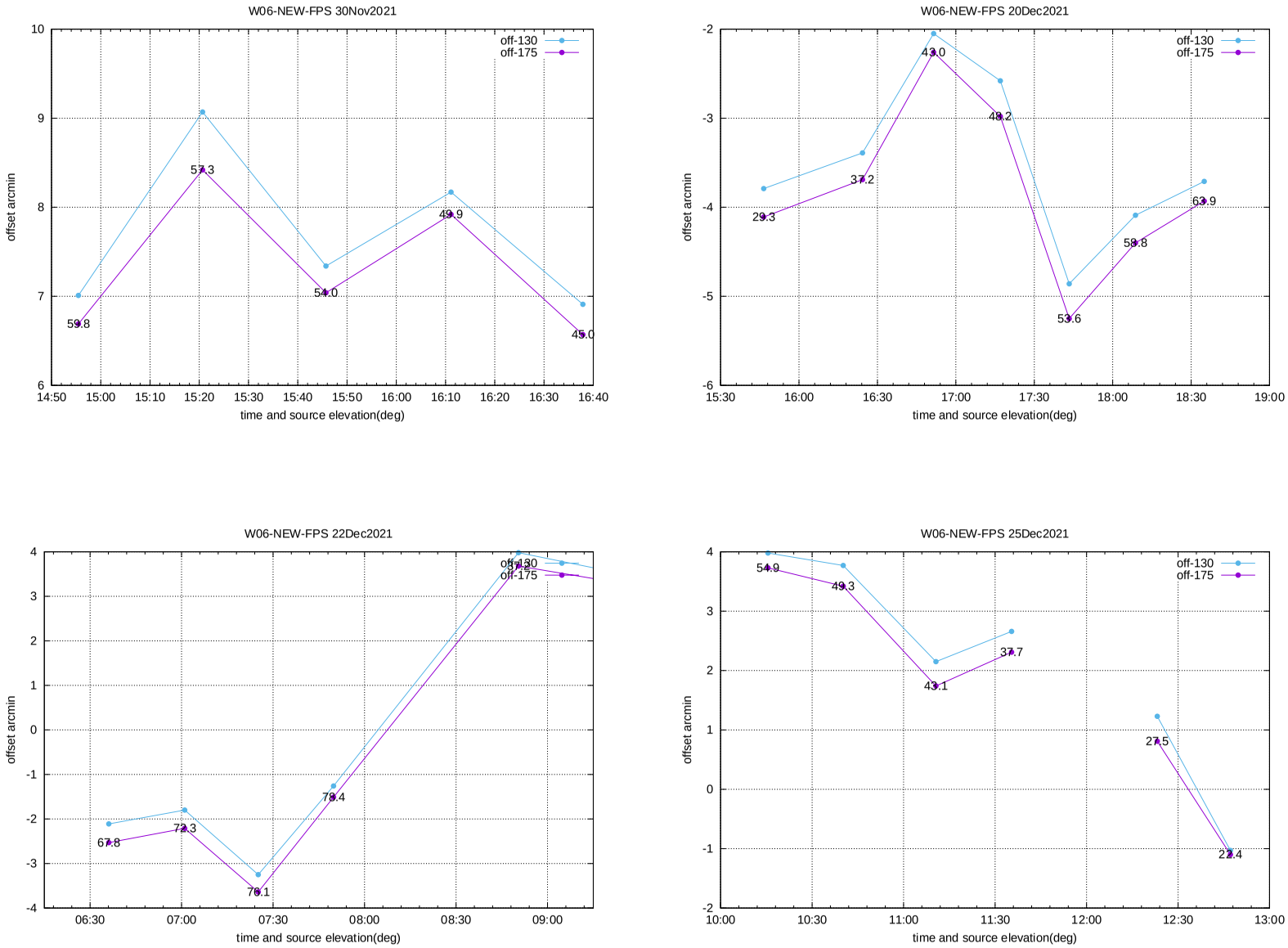

Antenna elevation offset as a function of time and elevation (shown against each points).

Figure 29: Elevation offsets after each `feed-rotation`.

to change significantly at low elevation, and the $\sim 2'$ offset seen for the last 2 scans at low elevation is believed to be caused by gravitational bending of the antenna.

On 20th December, the elevation angle changed from 29 to 64° during feed rotations. Except for C01 (Fig. 2), W02 (Fig. 25) and W03 (Fig. 26), change in antenna based elevation offsets involving antennas with new FPS systems remained within $\sim 1'$ from their mean positions. Sixth scan involving antenna C01 shows a jump in offset (as expected from error in feed positioning). However, closer examination of the particular scan done with grid-pointing showed Gaussian fit to have failed. This antenna is known to have the maximum elevation dependant pointing error among all the antennas, and systematic change in offset with elevation by $\sim 4'$ is believed to be caused by that. Like C11 (30th Nov), 2nd scan of W02 showed jump in pointing offset (Fig. 25). However, no problem was seen for grid-pointing for this scan. This was also likely caused by failure of new FPS to position the feed in automatic mode. The same problem has repeated on W03 on the same day(Fig. 26).

On 22nd Dec, elevation angle changed from 68° to 78° while observing 3C286 for the band-5 scans. The last scan shown was while observing the calibrator 1459+716, and the elevation angle was 37°. The large change in elevation angle for the last scan is believed to have caused change in elevation offsets by several arc-mins for C01 (Fig. 2), C02 (Fig. 3), C05 (Fig. 6), S06 (Fig. 23) and W06 (Fig. 29). Third scan of W02 (Fig. 25) and fourth scan of W04 (Fig. 27) showed significant jump in pointing offsets. For W02, no problem was seen with grid-pointing for the 3rd scan. This was also likely caused by failure of new FPS to position the feed correctly in automatic mode. However, W04 was not working during the 4th scan, and the fit was bad, and it caused a jump in offset (not real). C10 (Fig. 9), C11 (Fig. 10), C13 (Fig. 12) and E06 (Fig. 18) offset changed systematically with elevation indicating gravitational bending to be the cause.

3.2 Weekly pointing tests with fixed offsets

3.2.1 May-Jul 2022

Attached are the plots (figures 31−35) of pointing offsets as a function of epochs of observations (in weeks starting from 05th May) between 05th May to 28th July 2022. The '+' symbols in Pink colour show the stratospheric refraction subtracted elevation offsets. We also show the offsets ('X' symbols) in Green colour after subtracting the expected variation of pointing error (as a function of elevation and azimuth using the pointing model of May 2022) with a DC offset [determined from f(x)=C fit] for each antennas. We determined the standard error (FIT_STDFIT) of the fits by assuming an rms error of $1'$ in offsets for all the antennas (Table 1, page-40).

If all the antennas had rms pointing error of $1'$, then the standard error would be unity. However, as shown in Table-1 (page-40) two of the antennas show standard-errors of the fits > 2, indicating rms pointing error of $\gtrsim 2'$ for S06 and W06. Also, C00, C02, C04, C05 (Fig. 24) and W05 had rms pointing error $\sim 1.5'$. Among these antennas, C00, C04, C05 (Fig. 31), S06 (Fig. 34) and W05 (Fig. 35) show systematic variation of offsets, which suggests offset variation due to change of elevation and azimuth from an week to the next, which the pointing model could not account properly. C02 show bulk of the variation to occur from 2 weeks of offsets (week 3 & 4) to be different from the other days of observations. For W06, last 3 weeks of offsets are different from the rest. It appears that the antenna offset changed during the 3 weeks, for which there was no data from this antenna.

3.2.2 November 2022 - February 2023

Attached below are the plots of pointing offsets as a function of epochs of observations (in weeks) between 17th November 2022 to 23rd February 2023 (figures 36−40). The '+' symbols in Pink colour show the stratospheric refraction subtracted elevation offsets. We also show the offsets ('X' symbols) in Green colour after subtracting the expected variation of pointing error (as a function of elevation and azimuth using the latest pointing model of May 2022) with a DC offset [determined from f(x)=C

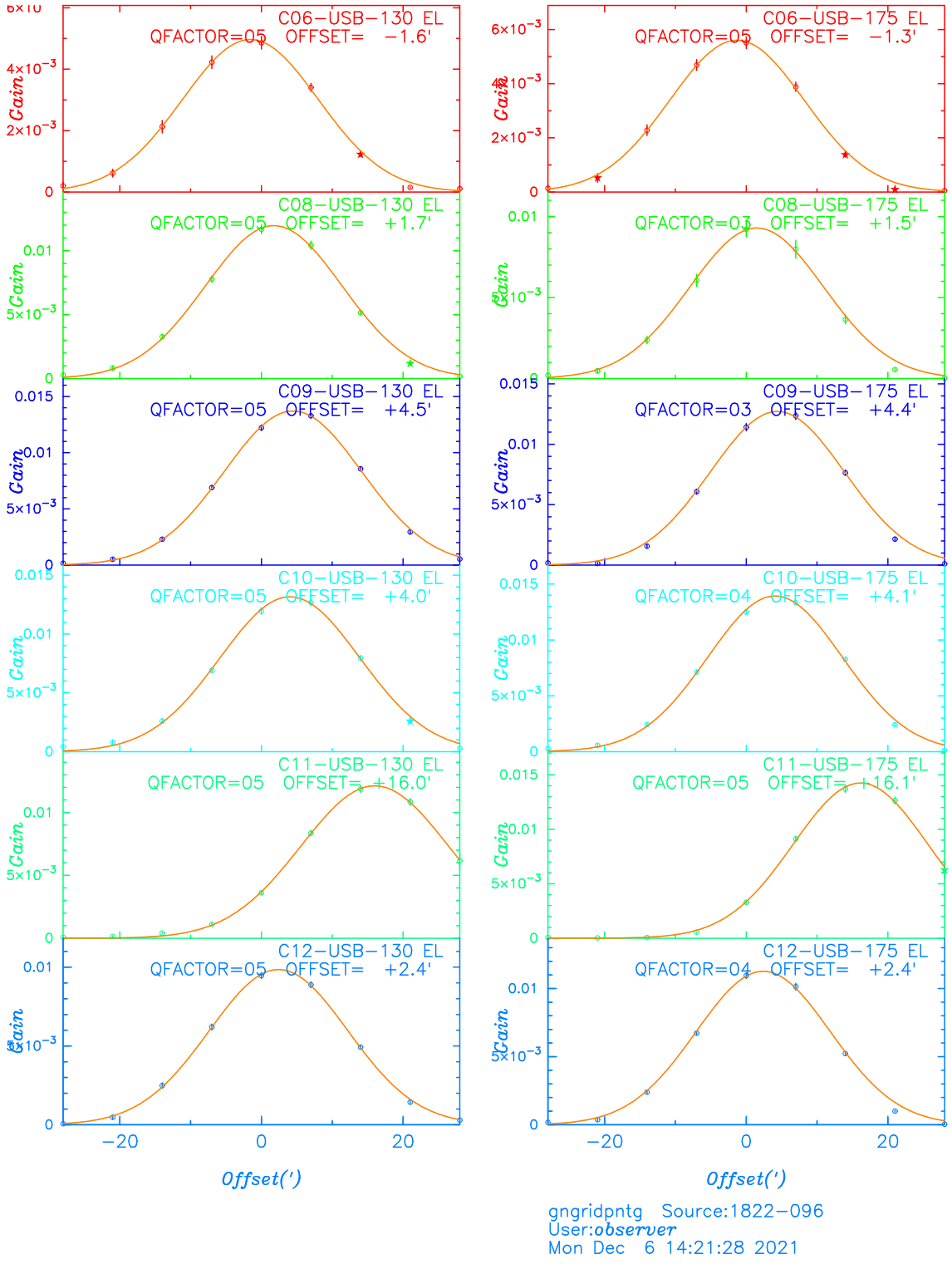

Figure 30: Gaussian fits to elevation grid-pointing data for the antennas C6−C12 on 30th Nov 2021

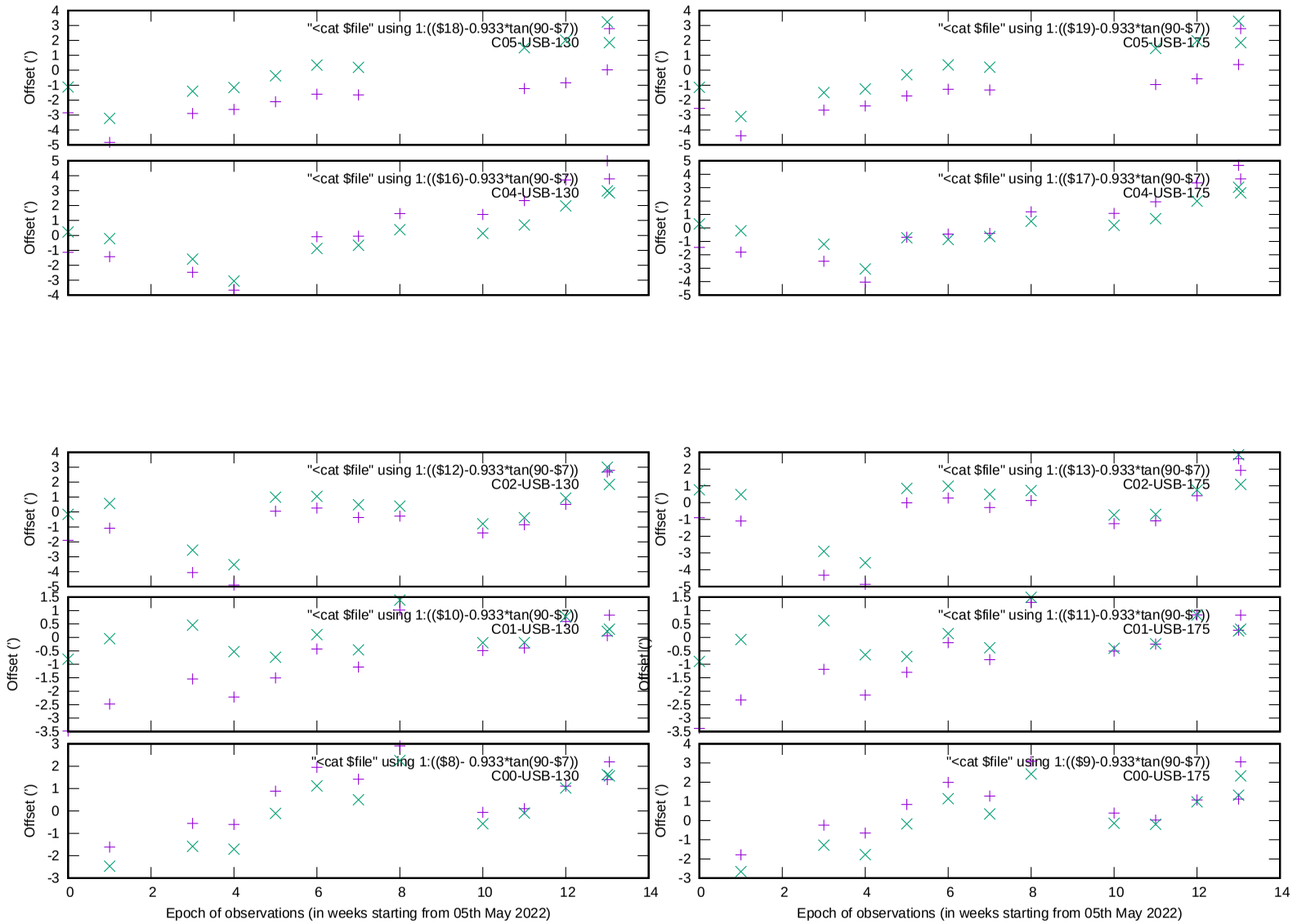

Figure 31: Elevation offsets from weekly pointing after loading `fixed offsets`.

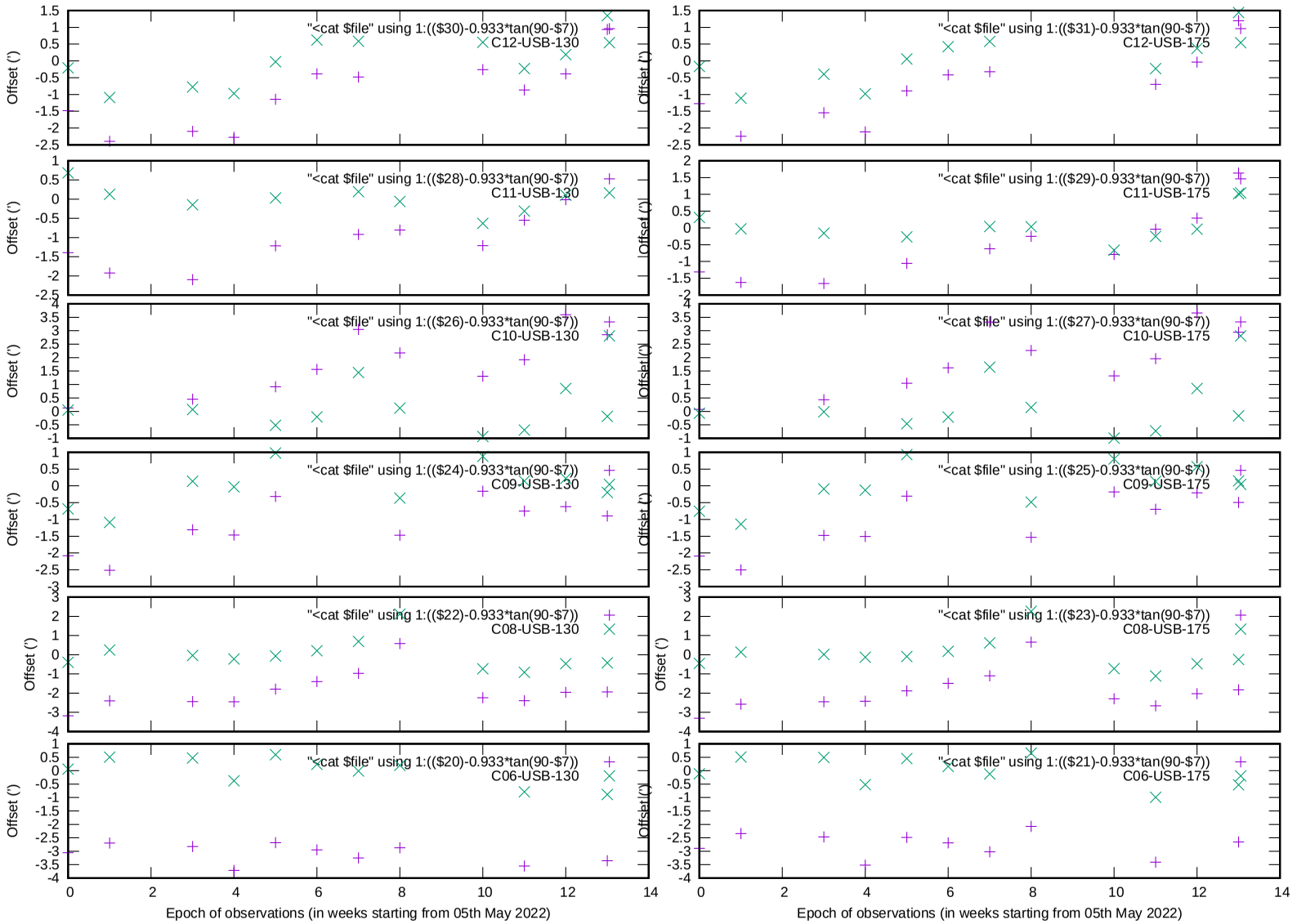

Figure 32: Elevation offsets from weekly pointing after loading `fixed offsets`.

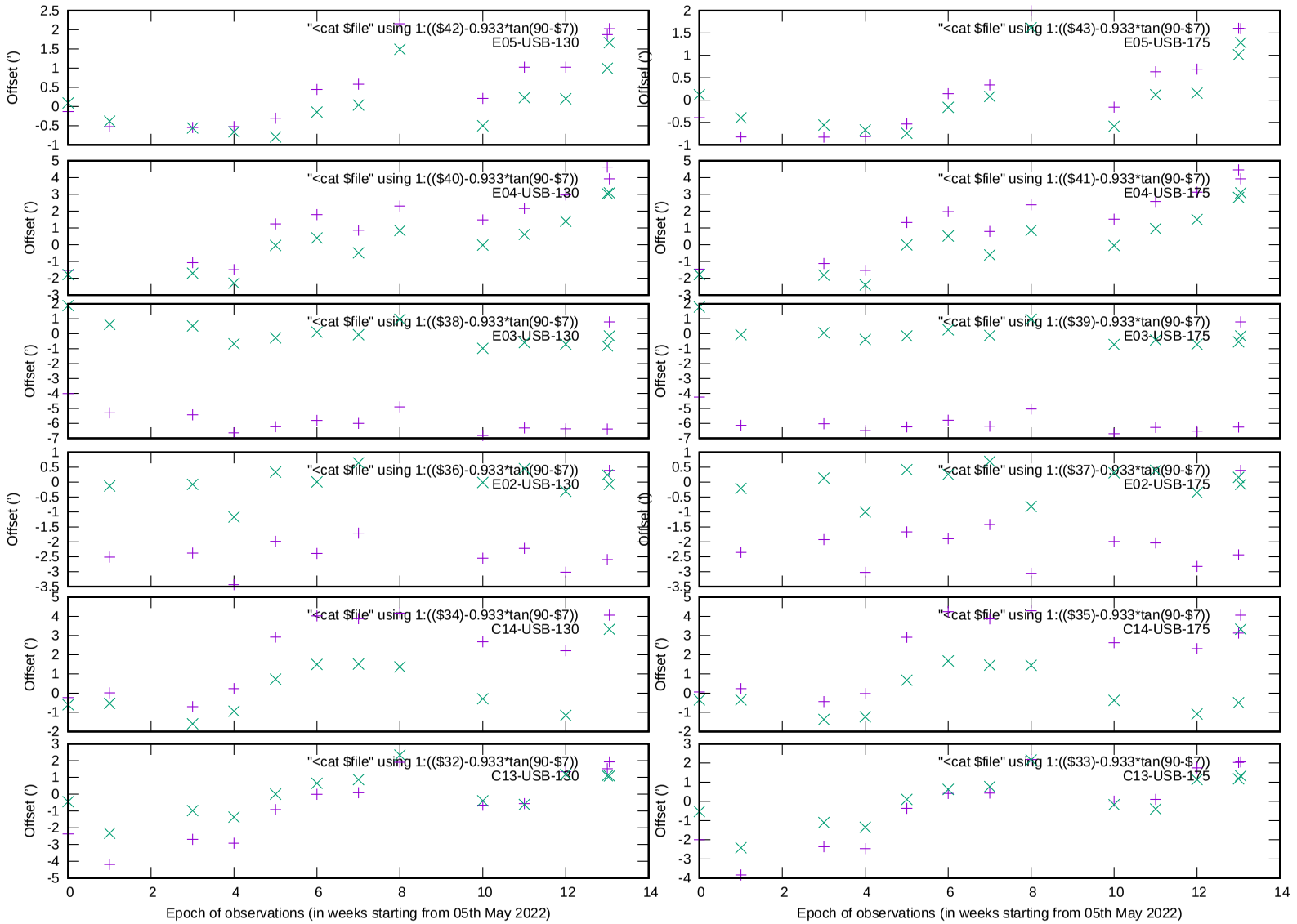

Figure 33: Elevation offsets from weekly pointing after loading `fixed offsets`.

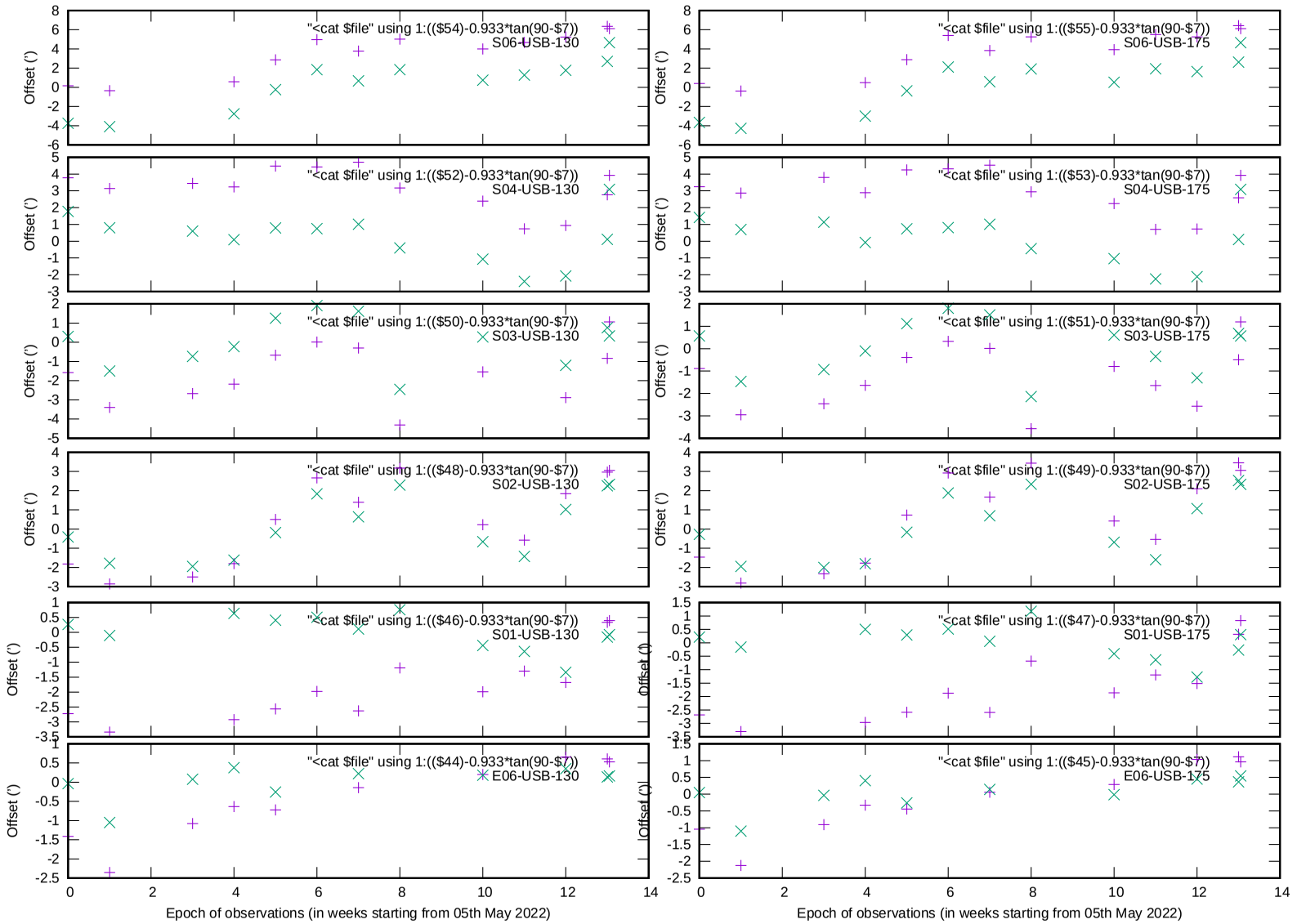

Figure 34: Elevation offsets from weekly pointing after loading `fixed offsets`.

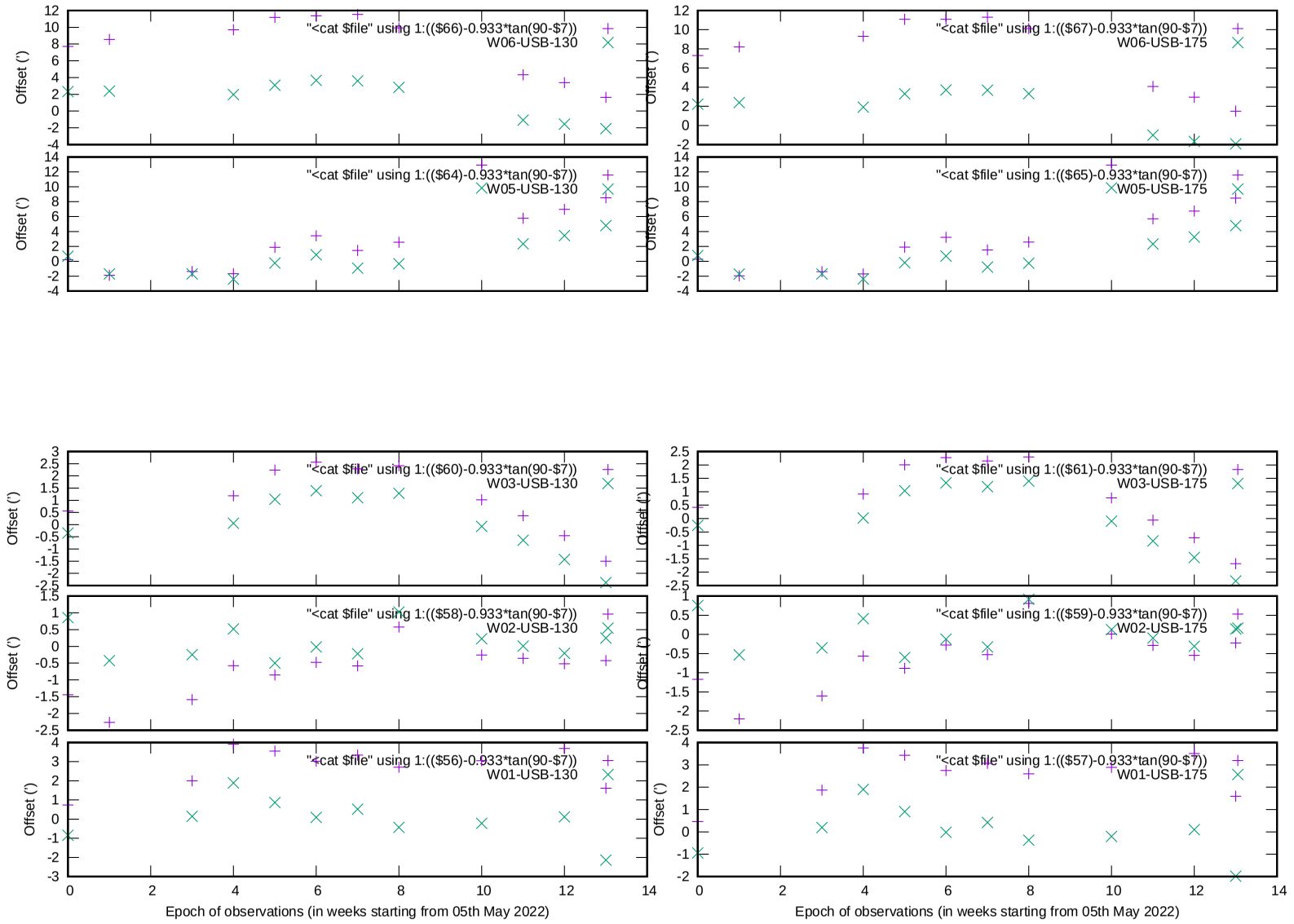

Figure 35: Elevation offsets from weekly pointing after loading `fixed offsets`.

Table-1: Standard error on DC offsets after model subtraction from pointing data

Antenna_name-Poln	FIT_STDFIT (Average EL Std-error=1.1')
C00-USB-130	Std-error= 1.48
C00-USB-175	Std-error= 1.48
C01-USB-130	Std-error= 0.64
C01-USB-175	Std-error= 0.70
C02-USB-130	Std-error= 1.71
C02-USB-175	Std-error= 1.76
C03-USB-130	Std-error= NaN
C03-USB-175	Std-error= NaN
C04-USB-130	Std-error= 1.63
C04-USB-175	Std-error= 1.55
C05-USB-130	Std-error= 1.88
C05-USB-175	Std-error= 1.87
C06-USB-130	Std-error= 0.52
C06-USB-175	Std-error= 0.54
C08-USB-130	Std-error= 0.79
C08-USB-175	Std-error= 0.84
C09-USB-130	Std-error= 0.63
C09-USB-175	Std-error= 0.66
C10-USB-130	Std-error= 0.71
C10-USB-175	Std-error= 0.76
C11-USB-130	Std-error= 0.36
C11-USB-175	Std-error= 0.43
C12-USB-130	Std-error= 0.75
C12-USB-175	Std-error= 0.75
C13-USB-130	Std-error= 1.28
C13-USB-175	Std-error= 1.26
C14-USB-130	Std-error= 1.17
C14-USB-175	Std-error= 1.12
E02-USB-130	Std-error= 0.50
E02-USB-175	Std-error= 0.53
E03-USB-130	Std-error= 0.86
E03-USB-175	Std-error= 0.73
E04-USB-130	Std-error= 1.55
E04-USB-175	Std-error= 1.56
E05-USB-130	Std-error= 0.68
E05-USB-175	Std-error= 0.70
E06-USB-130	Std-error= 0.43
E06-USB-175	Std-error= 0.47
S01-USB-130	Std-error= 0.62
S01-USB-175	Std-error= 0.65
S02-USB-130	Std-error= 1.57
S02-USB-175	Std-error= 1.68
S03-USB-130	Std-error= 1.37
S03-USB-175	Std-error= 1.25
S04-USB-130	Std-error= 1.26
S04-USB-175	Std-error= 1.23
S06-USB-130	Std-error= 2.41*
S06-USB-175	Std-error= 2.50*
W01-USB-130	Std-error= 1.06
W01-USB-175	Std-error= 1.03
W02-USB-130	Std-error= 0.41
W02-USB-175	Std-error= 0.48
W03-USB-130	Std-error= 1.25
W03-USB-175	Std-error= 1.27
W04-USB-130	Std-error= NaN
W04-USB-175	Std-error= NaN
W05-USB-130	Std-error= 1.86
W05-USB-175	Std-error= 1.80
W06-USB-130	Std-error= 2.18*
W06-USB-175	Std-error= 2.13*

fit] for each antennas. We determined the standard error (FIT_STDFIT) of the fits by assuming an rms error of $1'$ in offsets for all the antennas (Table 2, page-47).

If all the antennas had rms pointing error of $1'$, then the standard error would be unity. Unlike the previous epoch (section 3.2.1), none of the antennas show standard-error of the fits to be >2. However, S04, W03 and W05 had standard error $\sim 1.5-2$ (Table 2, page-47). Among these antennas, S04 (Fig. 39) did not work for half the days, and offset of the last epoch after a gap of 4 weeks from last measurement is different from the rest. W03 and W05 (Fig. 39) show systematic variation of offsets, which suggests the pointing offset variation to be due to change of elevation and azimuth from an week to the next, which the pointing model could not account properly.

4 Discussions

During 1st part of the tests (multiple feed rotations followed by grid pointing), for out of a total of ∼700 grid-pointings in elevation involving all antennas, we could identify 4 cases, where feed rotation with the new FPS appeared to have failed to reach an accuracy of $10'$. This caused pointing error $> 1'$ (ratio of feed rotation offset to antenna pointing offset is 10:1 for GMRT), when script based automatic feed rotation was used to rotate the feeds to their desired position. However, these isolated cases were believed to be due to occasional problems with automatic feed rotation, where the feed fails to reach the desired angular position. The system on query did indicate the failure (on 30th Nov 2021), and it could be focused as expected by sending commands later. It should not affect regular feed rotation under manual supervision.

The 2nd part of the tests (weekly pointing tests with fixed offsets) as described in sections 3.2.1 & 3.2.2, there are several antennas that show rms point-errors well above $1'$. However, most of these antennas show significant variation in a systematic fashion across the time-spans of observations, suggesting the variation to be due to changes of antenna offsets with changes in elevation and azimuth, which the pointing model could not account properly. Only 3 antennas (C2 & W06 during May−July 2022 and S04 during November 22 − February 23) showed significant change/jump in pointing offsets between 2 consecutive observations. However, two of the antennas (S04 & W06) had large gaps of several weeks between the 2 measurements, over which the antennas did not work during the weekly pointing observations. The observed change in pointing offsets after the time gaps could be due to comparatively large change in elevation and azimuth of the source during observations over the above timescales ($\sim$ 1-month). Also, during that time, certain mechanical activities on the antennas could have been taking place, which could change the fixed offsets of the antennas (e.g., encoders). In an earlier report (Roy 2021, available from http://library.ncra.tifr.res.in:8080/jspui/handle/2301/517), we applied the pointing model that was derived from June 2019 observations to four different pointing observations done between 2017 to 2020. The standard errors of the fits are shown in Table-3 (page-48). The number of antennas with high (>2) and moderate (between 1.5 and 2) standard errors are seen to be comparable with the results presented above in Table-1 & 2.

Therefore, with feed rotation using the new absolute FPS (without doing pointing after feed rotation), the pointing performance appears to be the same as before, where, pointing offsets were needed to be measured through astronomical pointing tests after every feed rotation and were corrected for. The rms error of pointing remains $\sim 1'$ in general.

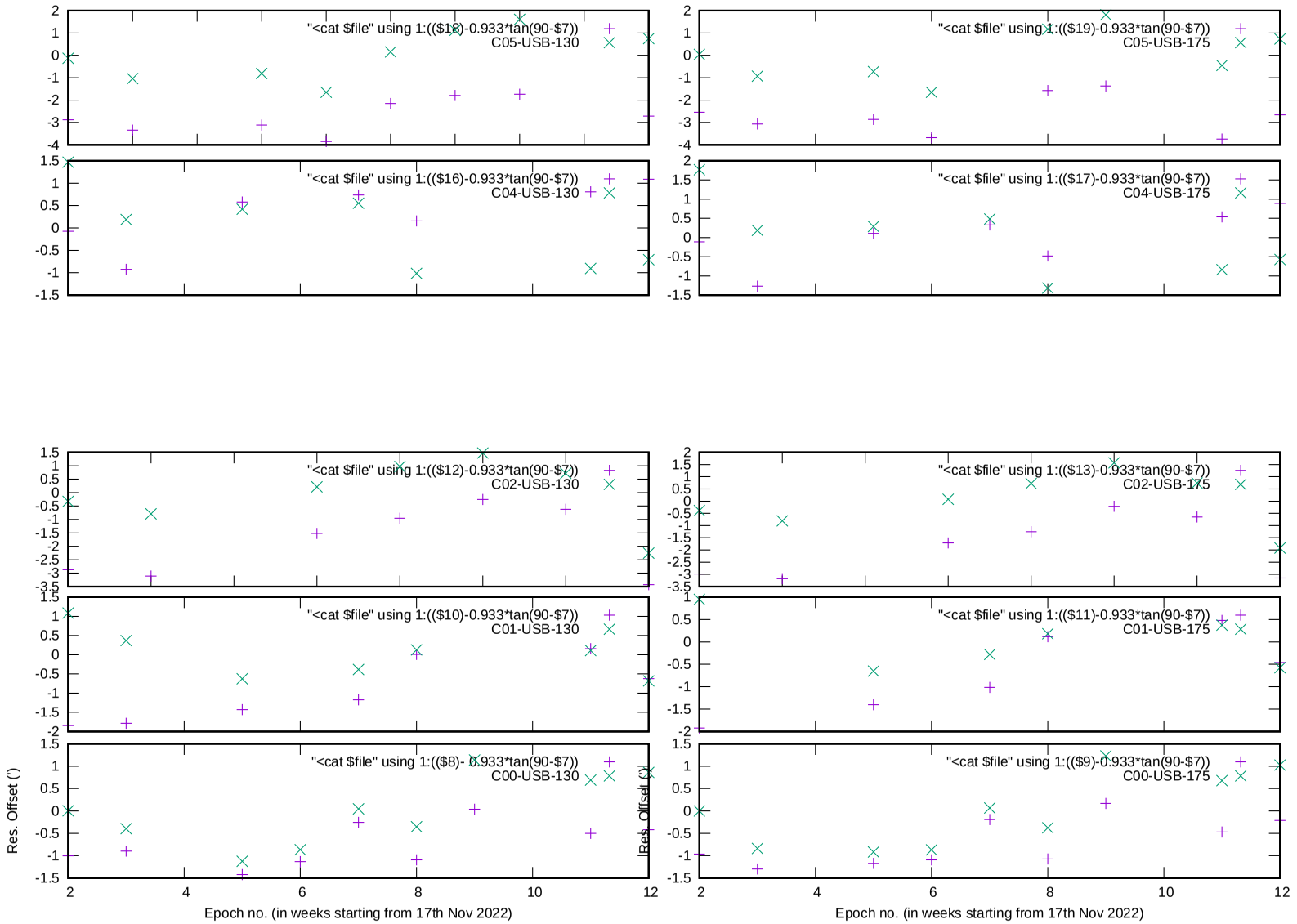

Figure 36: Elevation offsets from weekly pointing after loading `fixed offsets`.

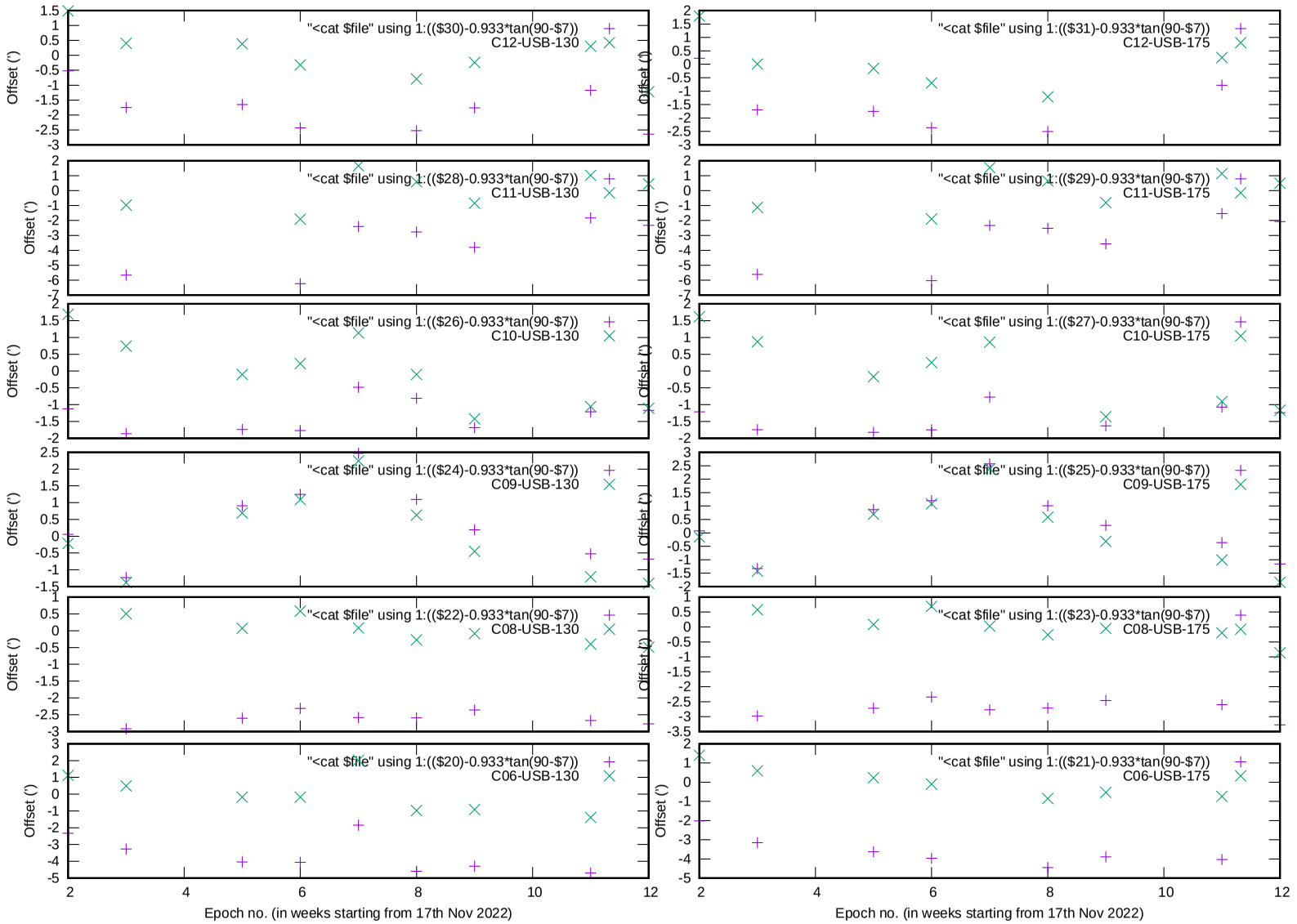

Figure 37: Elevation offsets from weekly pointing after loading `fixed offsets`.

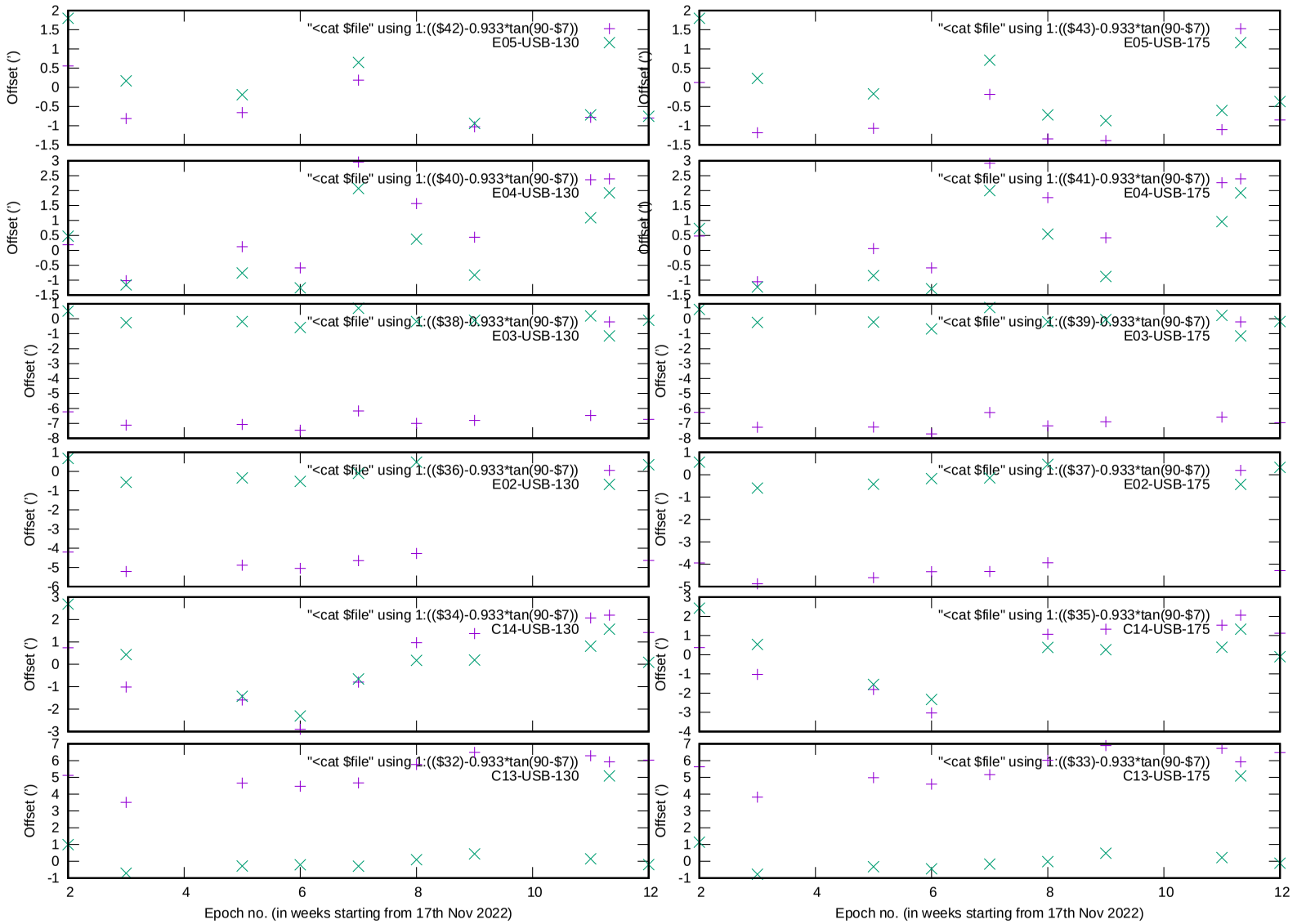

Figure 38: Elevation offsets from weekly pointing after loading `fixed offsets`.

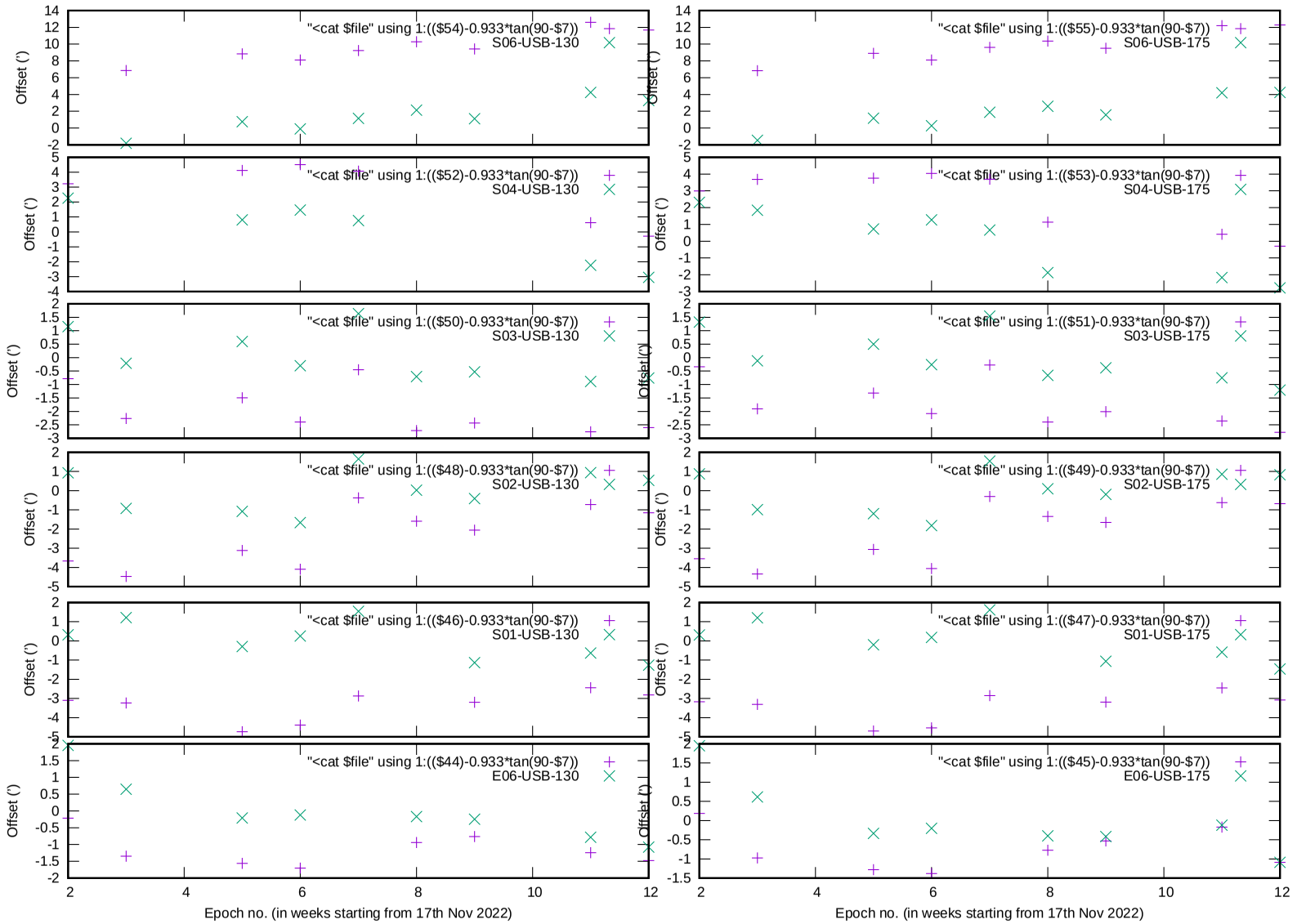

Figure 39: Elevation offsets from weekly pointing after loading `fixed offsets`.

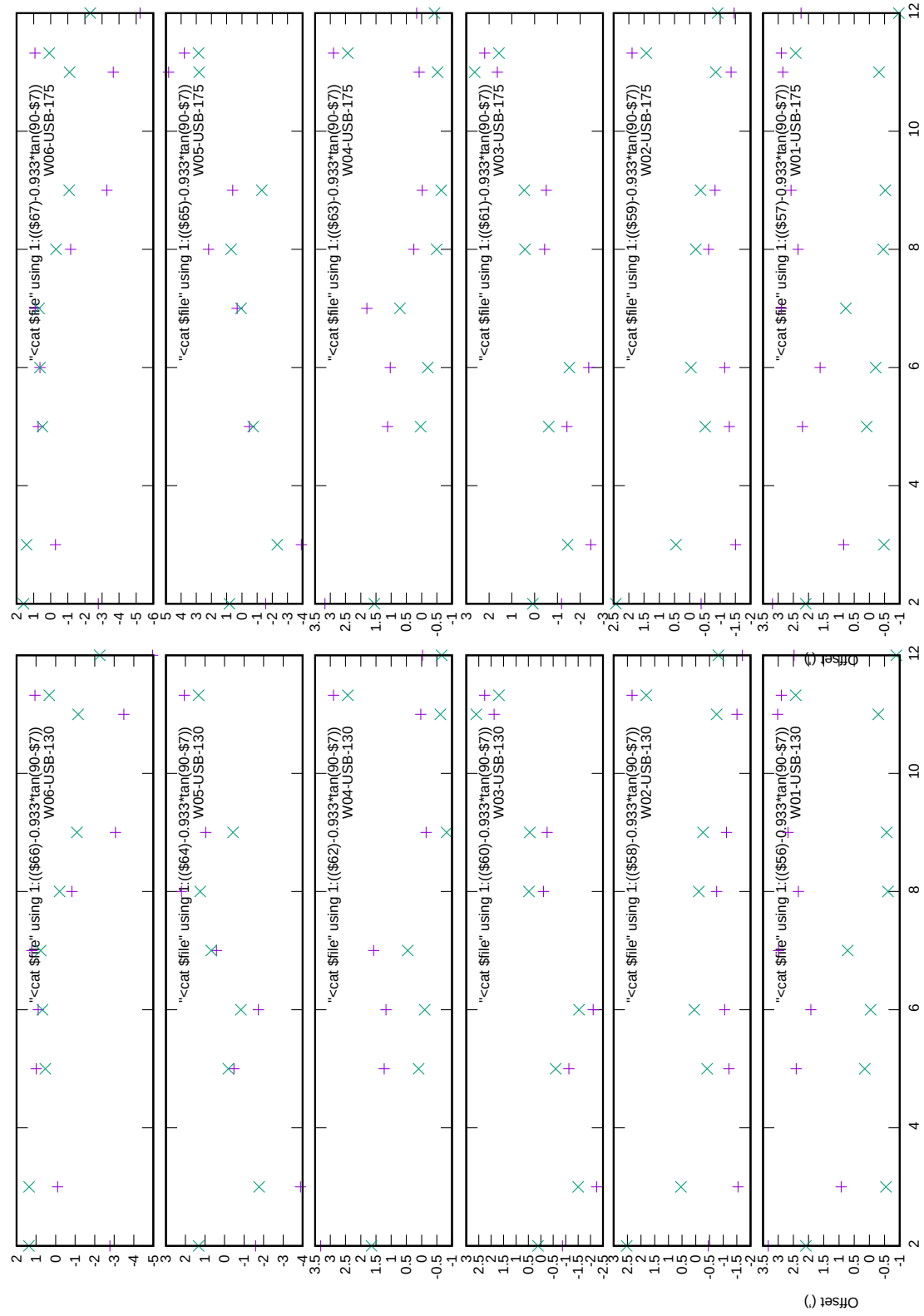

Figure 40: Elevation offsets from weekly pointing after loading `fixed offsets`.

Table-2
Standard error on DC offsets after model subtraction from EL pointing data

Antenna_name-Poln	FIT_STDFIT
C00-USB-130	Std-error= 0.77
C00-USB-175	Std-error= 0.82
C01-USB-130	Std-error= 0.62
C01-USB-175	Std-error= 0.59
C02-USB-130	Std-error= 1.21
C02-USB-175	Std-error= 1.13
C03-USB-130	Std-error= NaN
C03-USB-175	Std-error= NaN
C04-USB-130	Std-error= 0.92
C04-USB-175	Std-error= 1.00
C05-USB-130	Std-error= 1.06
C05-USB-175	Std-error= 1.09
C06-USB-130	Std-error= 1.28
C06-USB-175	Std-error= 0.91
C08-USB-130	Std-error= 0.51
C08-USB-175	Std-error= 0.55
C09-USB-130	Std-error= 1.19
C09-USB-175	Std-error= 1.27
C10-USB-130	Std-error= 1.01
C10-USB-175	Std-error= 1.01
C11-USB-130	Std-error= 1.27
C11-USB-175	Std-error= 1.19
C12-USB-130	Std-error= 0.81
C12-USB-175	Std-error= 0.95
C13-USB-130	Std-error= 0.47
C13-USB-175	Std-error= 0.55
C14-USB-130	Std-error= 1.41
C14-USB-175	Std-error= 1.52
E02-USB-130	Std-error= 0.75
E02-USB-175	Std-error= 0.62
E03-USB-130	Std-error= 0.38
E03-USB-175	Std-error= 0.43
E04-USB-130	Std-error= 1.13
E04-USB-175	Std-error= 1.15
E05-USB-130	Std-error= 0.95
E05-USB-175	Std-error= 0.88
E06-USB-130	Std-error= 0.90
E06-USB-175	Std-error= 0.89
S01-USB-130	Std-error= 1.02
S01-USB-175	Std-error= 1.05
S02-USB-130	Std-error= 1.05
S02-USB-175	Std-error= 1.12
S03-USB-130	Std-error= 0.87
S03-USB-175	Std-error= 0.89
S04-USB-130	Std-error= 1.95 (Jump in reading
S04-USB-175	Std-error= 1.84 after 7th week).
S06-USB-130	Std-error= 1.31
S06-USB-175	Std-error= 1.33
W01-USB-130	Std-error= 0.92
W01-USB-175	Std-error= 0.92
W02-USB-130	Std-error= 1.20
W02-USB-175	Std-error= 1.17
W03-USB-130	Std-error= 1.78
W03-USB-175	Std-error= 1.80
W04-USB-130	Std-error= 0.81
W04-USB-175	Std-error= 0.76
W05-USB-130	Std-error= 1.14
W05-USB-175	Std-error= 1.67
W06-USB-130	Std-error= 1.40
W06-USB-175	Std-error= 1.46

Table-3

Standard error on DC offsets after Jun19 model subtraction from EL pointing data

Antenna-Pol	23Aug17	03Mar19	14Nov19	02Dec20
C00-USB-130	1.98*	1.23	1.33	1.24
C00-USB-175	2.00*	1.28	1.38	1.25
C01-USB-130	1.17	0.80	1.26	1.39
C01-USB-175	1.14	0.82	1.29	1.33
C02-USB-130	0.95	1.03	0.67	0.67
C02-USB-175	1.05	1.07	0.67	0.67
C03-USB-130	0.6	1.77	0.67	NaN
C03-USB-175	0.63	1.74	0.61	NaN
C04-USB-130	0.53	1.25	0.67	1.87
C04-USB-175	0.52	1.24	0.61	1.86
C05-USB-130	0.86	0.75	0.7	NaN
C05-USB-175	0.89	0.62	0.74	NaN
C06-USB-130	0.45	0.91	0.64	0.78
C06-USB-175	0.47	0.86	0.64	0.8
C08-USB-130	0.74	0.8	0.59	NaN
C08-USB-175	0.67	0.95	0.64	NaN
C09-USB-130	1.04	1.27	1.17	1.04
C09-USB-175	1.03	1.22	1.14	1.03
C10-USB-130	1.00	1.77	1.14	0.88
C10-USB-175	0.96	1.75	1.06	0.83
C11-USB-130	0.56	0.84	0.93	0.56
C11-USB-175	0.59	0.85	0.87	0.63
C12-USB-130	0.3	0.71	0.48	0.45
C12-USB-175	0.31	0.69	0.47	0.36
C13-USB-130	0.91	1.15	0.92	0.93
C13-USB-175	0.9	1.10	0.92	0.93
C14-USB-130	NaN	1.04	1.10	1.55
C14-USB-175	NaN	0.97	1.07	1.62
E02-USB-130	0.61	0.9	0.74	0.85
E02-USB-175	0.64	0.90	0.71	0.88
E03-USB-130	1.01	1.18	1.14	1.18
E03-USB-175	1.00	1.15	1.09	1.14
E04-USB-130	0.51	0.83	0.51	0.8
E04-USB-175	0.50	0.84	0.52	0.78
E05-USB-130	0.71	0.90	NaN	1.04
E05-USB-175	0.73	0.90	NaN	0.99
E06-USB-130	0.38	0.72	0.28	0.50
E06-USB-175	0.38	0.74	0.3	0.44
S01-USB-130	0.42	0.83	0.5	0.53
S01-USB-175	0.60	0.85	0.60	0.51
S02-USB-130	1.94*	1.78	2.13*	2.03*
S02-USB-175	1.95*	1.79	2.14*	2.00*
S03-USB-130	0.81	0.85	0.64	0.72
S03-USB-175	0.83	0.89	0.67	0.72
S04-USB-130	0.50	0.9	0.31	NaN
S04-USB-175	0.50	0.97	0.38	NaN
S06-USB-130	2.18*	2.28*	3.10*	2.38*
S06-USB-175	2.20*	2.32*	3.11*	2.40*
W01-USB-130	1.31	1.64	1.2	1.04
W01-USB-175	1.29	1.61	1.18	1.00
W02-USB-130	0.77	1.1	0.6	0.59
W02-USB-175	0.75	1.10	0.6	0.61
W03-USB-130	1.50	1.46	1.38	1.45
W03-USB-175	1.4	1.45	1.26	1.41
W04-USB-130	1.08	1.14	1.17	1.06
W04-USB-175	1.07	1.16	1.16	1.04
W05-USB-130	1.12	1.47	1.00	0.96
W05-USB-175	1.12	1.51	1.00	1.01
W06-USB-130	1.14	1.37	1.20	0.43
W06-USB-175	1.13	1.38	1.16	0.45